A General Algorithm for Exact Simulation of Multicomponent Aggregation Processes

Ian J. Laurenzi,[*,1] John D. Bartels,[†] and Scott L. Diamond[*,1]

Department of Chemical Engineering, Institute for Medicine and Engineering, University of Pennsylvania, Philadelphia, Pennsylvania 19104; and †NOMOS Corporation, Sewickley, Pennsylvania 15143

E-mail: laurenzi@seas.upenn.edu, bartej2@rpi.edu, and sld@seas.upenn.edu

A Monte Carlo (MC) algorithm is presented for the simulation of the time evolution of aggregation processes featuring multiple components, properties, or conservation laws. Instead of using deterministic differential population balance equations, the MC algorithm utilizes a stochastic approach to aggregation kinetics. As a result, exact simulation of spatially independent aggregation processes is possible without the need for numerical approximations. Furthermore, simulations exactly predict all moments of the size and composition distributions of aggregating particles for both nongelling and gelling kernels and extend these results to the postgelation period. The algorithm is shown to require at most $O\left((\Omega_1 \Omega_2 \ldots \Omega_\kappa)^{1/(\kappa+1)}\right)$ rate-limiting operations per time step for a κ-component aggregation process featuring Ω_i monomers of each component i—a substantial performance improvement over the potential of previous methods. Simulation results are presented for bivariate sum, product, and constant kernels, and for the perikinetic (Brownian) kernel. © 2002 Elsevier Science (USA)

Key Words: coagulation; clustering; collection; moments; gel transition.

1. INTRODUCTION

The process of aggregation is ubiquitous in nature and underlies many scientific, medical, and industrial research areas and applications. Often, aggregating particles are not isotropic in composition but are composed of several components. Examples of such heterotypic processes include copolymerization and the coagulation of blood, where many types of chemical monomers or cells polymerize or aggregate according to their respective affinities for each other. In such processes, knowledge of both the size *and* composition of aggregating particles is often critical to the successful prediction of their time evolution. For example, blood coagulation is strongly dependent on both the relative and

---

[1] Fax: (215) 573-7227.

absolute concentrations of leukocytes and platelets, on soluble fibrinogen, and on other blood components.

The kinetics of spatially homogeneous multicomponent aggregation processes are usually described by population balance equations (PBEs) such as

$$\frac{\partial c(m, n; t)}{\partial t} = \frac{1}{2} \sum_{m'=0}^{m} \sum_{n'=0}^{n} K(m - m', n - n' \mid m', n') c(m - m', n - n'; t) c(m', n'; t)$$

$$- c(m, n; t) \sum_{m'=0}^{\infty} \sum_{n'=0}^{\infty} K(m, n \mid m', n') c(m', n'; t), \tag{1}$$

which have enjoyed vast success in their ability to predict the time evolution of the size distributions of aggregating particles. Originally derived from chemical considerations [25], PBEs give a deterministic description of the kinetics of a system of "polymerization reactions." Hence, Eq. (1) may be interpreted as a differential population balance for a two-component "copolymerization" where $c(m, n; t)$ is the expected concentration of m, n-mers and the kernels $K(k, \ell \mid m, n)$ are chemical rate constants for the reaction $A_k B_\ell + A_m B_n \to A_{k+m} B_{\ell+n}$. Although Eq. (1) describes discrete aggregation processes, it can be expanded in scope to describe aggregation processes featuring particles with arbitrary sizes to give Lushnikov's equation [16],

$$\frac{\partial \hat{c}(u, v; t)}{\partial t} = \frac{1}{2} \int_0^u \int_0^v K(u, v \mid u - u', v - v') \hat{c}(u', v'; t) \hat{c}(u - u', v - v'; t) \, dv' \, du'$$

$$- \hat{c}(u, v; t) \int_0^\infty \int_0^\infty K(u, v \mid u', v') \hat{c}(u', v', t) \, dv' \, du', \tag{2}$$

where $\hat{c}(u, v; t) \, du \, dv$ is the expected concentration of particles in the composition range $\{[u, u + du), [v, v + dv)\}$. Defining a cumulative particle composition distribution

$$G(u, v; t) = \int_0^u \int_0^v \hat{c}(u, v; t) \, dv \, du, \tag{3}$$

the expected concentration of particles on the component intervals $[u, u']$ and $[v, v']$ is given by

$$c([u, u'], [v, v']; t) = G(u', v'; t) - G(u, v; t). \tag{4}$$

Although written as single equations, PBEs such as Eqs. (1) and (2) represent potentially infinite sets of highly coupled nonlinear differential equations. As a result of this mathematical complexity, analytical solutions of multicomponent PBEs are known for only a few simple kernels [4, 12, 16]. This has been a cause for concern in transport-limited aggregation and copolymerization, where the kernels governing these real physical processes do not permit analytical solutions to their PBEs.

We have been careful to note that Eqs. (1) and (2) are deterministic equations for the description of the *expected values* of the concentrations of particle species. That is, they

describe the kinetics of aggregation processes in the thermodynamic limit and provide no information regarding their innate fluctuations. Although such equations are accurate for the description of systems with large numbers of particles, they cease to be accurate in the limit of complete aggregation, where the assumptions underlying deterministic treatment of kinetics become unrealistic as the particle populations become small [5, 20].

As with small systems of chemical reactants, these obstacles can be overcome by a probabilistic representation of the process [22]. In contrast to the deterministic approach, the stochastic approach to aggregation kinetics describes the time evolution of the process in terms of a stochastic master equation. In contrast to PBEs that specify the concentration of m, n-mers, a master equation specifies the *probability* $P(\mathbf{x}, t \mid \mathbf{x}_0, 0)$ that the system is in the state $\mathbf{x}$ at some time t, given that it was in some other state $\mathbf{x}_0$ at $t = 0$. In a two-component process as previously described, the state $\mathbf{x} = \{X_{m,n}\}$ is defined by a unique set of populations of all types of m, n-mers. The stochastic approach to aggregation kinetics is extremely robust, possessing the ability to describe the kinetics of aggregation processes in both the large and small population limits of aggregation processes [2, 5, 6, 9, 17, 20, 21]. Unfortunately, despite solutions of master equations for a few special cases of single-component aggregation processes [2, 9, 17, 27], there is no general solution method for master equations for multicomponent systems with arbitrary kernels. This motivates the present study.

The stochastic approach to aggregation kinetics has reemerged as an attractive alternative to the PBEs in recent years as a basis of Monte Carlo (MC) simulation [15, 24, 30]. In this context, the stochastic approach may be employed to determine both the expectation values and its fluctuations for multicomponent aggregation processes. In this work, we describe an exact and efficient MC algorithm for the simulation of the time evolution of any spatially homogeneous aggregation process with any number of components, or conservation laws. In addition, we demonstrate the ability of the algorithm to predict the dynamics of gelling systems in their postgelation phase, where the physics is dominated by the stochastic nature of small populations.

2. STOCHASTIC APPROACH TO AGGREGATION KINETICS

Instead of concerning itself with the solution of master equations, the MC realization of the stochastic approach focuses on the transitions to and from the potential states of the aggregating system, characterizing the process as a Markov chain. Consequently, the implementation of the approach strongly depends on the definition of the states of the system. One choice is to define the state of the system in terms of the individual particles. In this framework, the state of a κ-component system is defined by a set of particles $i \in [1, N]$ with properties or compositions $\mathbf{u}_i = (u_{1,i}, u_{2,i}, \ldots u_{\kappa,i})$. Here, $u_{k,i}$ need not solely represent the amount of "component" k in species i. Rather, it may represent any number of properties, such as kinetic energy, momentum, or surface area.

The Markov chain is defined by the transition probabilities connecting each potential state of the system. Here, the stoichiometry of aggregation serves a key role. As states can only change by one aggregation event at a time, the transition probabilities between most states are zero. That is, because only three particles (two "reactants" and a "product") are involved in aggregation events, many events are required to transform most states to most other states. Thus, the only nonzero transition probabilities from any state are the

probabilities of aggregation between pairs of particles, resulting in a very sparse transition matrix. Therefore, these transition probabilities may be defined as

Pr{a specific pair of particles i and j will aggregate in the next time interval δt}

$$= C(\mathbf{u}_i, \mathbf{u}_j)\delta t + O(\delta t). \tag{5}$$

Using the probabilistic description of the aggregation process conferred by Eq. (5), Gillespie [6] developed particle-based MC simulation algorithms that serve as the bases of most other implementations of the stochastic approach [24, 26]. In these algorithms, a single state is stored in the computer memory and evolved probabilistically according to a "coalescence probability density function" $P(\tau, i, j)\,d\tau$ for the imminently aggregating particles ($i \in [1, N-1]$ and $j \in [i+1, N]$) and the quiescence time τ preceding their aggregation. Because this density function $P(\tau, i, j)$ may be derived from Eq. (5) without approximation, the results of stochastic simulations based upon it are both exact and complete. Moreover, quantitative information regarding both the mean behavior and fluctuations of the aggregation process can be obtained from the results of multiple simulations. Unfortunately, these particle accounting algorithms can be computationally demanding. For instance, a system of N particles requires storage for $N(N+1)/2$ transition probabilities given by Eq. (5) and requires at least $O(N)$ numerical operations per aggregation event. Therefore, computational storage and speed strongly limit the applicability of these algorithms to simulations with large numbers of particles.

These numerical difficulties may be curtailed significantly by adopting a different definition of the state of the system. The optimal choice follows from a chemical paradigm, whereby the state of the system is described in terms of the populations of aggregate *species*. As Eq. (1) defines a state by a set of species characterized as aggregates of $\{m, n\} \in \mathbb{N}^2$ monomers with concentrations $c(m, n; t) \in \mathbb{R}$, and Eq. (2) defines a state as a unique value of $G(u, v; t) \in \mathbb{R}$ for every $\{u, v\} \in \mathbb{R}^2$, we define states as ensembles of species $\mu \in [1, M]$ defined by unique properties or compositions $\mathbf{u}_\mu = (u_{1,\mu}, u_{2,\mu}, \ldots u_{\kappa,\mu})$ with populations $X_\mu \in \mathbb{N}$. For example, in a single-component discrete aggregation process initially containing 1000 monomers in some volume V, one state may be characterized by 1000 1-mers, another by 900 1-mers and 50 2-mers, and so forth. This definition expands on a mathematically similar concept developed by Spouge [26] for reducing the memory requirements of Gillespie's algorithm, although he did not expound the chemical context.

In addition to simplifying the accounting necessary for the state space, the "chemically" defined state space naturally lends itself to analysis by the stochastic approach to chemical kinetics [22]. In this context, the probabilities of "aggregation reactions" between species may be exactly defined as

Pr{a specific pair of particles of species μ and ν will aggregate in the next time interval δt}

$$= C(\mathbf{u}_\mu, \mathbf{u}_\nu)\delta t + O(\delta t). \tag{6}$$

The similarity of Eqs. (5) and (6) is no coincidence, as both probabilities pertain to the interaction of individual particles. However, the definition of the species-based state vector requires that the transition probabilities consider the number of ways two particles of species μ and ν may aggregate. Hence, the transition probabilities for a species-based state

space are

$$a(\mu, v)\, dt = C\,(\mathbf{u}_\mu, \mathbf{u}_v) X_\mu X_v\, dt$$

$$= \text{Pr}\{any \text{ two particles of } unlike \text{ species } \mu \text{ and } v \text{ with}$$

$$\text{populations } X_\mu \text{ and } X_v \text{ will aggregate in the next } dt\} \qquad (7)$$

and

$$a(\mu, \mu)\, dt = C\,(\mathbf{u}_\mu, \mathbf{u}_\mu) \binom{X_\mu}{2} dt$$

$$= \text{Pr}\{any \text{ two particles of } same \text{ species } \mu \text{ with}$$

$$\text{populations } X_\mu \text{ will aggregate in the next } dt\}. \qquad (8)$$

As the microphysics of an aggregation process are inbued in the PBE via the rate kernels, the quantities $C\,(\mathbf{u}_\mu, \mathbf{u}_v)$ clearly possess the same role in the stochastic approach. As it turns out, because PBEs such as Eqs. (1) and (2) may be derived from both stochastic considerations of particle collision [5, 21] and by consideration of stoichiometry in the derivation of chemical rate expressions for polymerizing systems [15], these rate kernels and probability densities for aggregation events are related by [5, 7]

$$C\,(\mathbf{u}_\mu, \mathbf{u}_v) \equiv \frac{K\,(\mathbf{u}_\mu, \mathbf{u}_v)}{V}. \qquad (9)$$

Equation (9) may be interpreted in the context of PBEs as follows: if species μ is defined by the composition $\mathbf{u}_\mu = (u, v)$ and species v by $\mathbf{u}_v = (u', v')$, then $K\,(\mathbf{u}_\mu, \mathbf{u}_v) = K\,(u, v \mid u', v')$, as in Eq. (2). Because the mathematical forms of rate kernels $K\,(\mathbf{u}_\mu, \mathbf{u}_v)$ derive from the laws of chemical kinetics and transport phenomena [3, 29], the stochastic approach to aggregation kinetics has a rigorous microphysical basis in addition to its theoretical completeness. Moreover, Eqs. (5)–(8) accomodate any kernel, including those explicitly dependent on time.

Using these transition probabilities, a general "aggregation probability density function" $P\,(\mu, v; \tau)\, d\tau$ may be defined, akin to the aforementioned "coalescence probability density function" utilized by Gillespie's particle-based methods. We define this quantity as

$$P\,(\mu, v; \tau)\, d\tau = \text{Pr}\{\text{two particles of species } \mu \text{ and } v \text{ will aggregate}$$

$$\text{after an interval of quiescence } \tau\}$$

$$= P_0(t + \tau \mid t)a(\mu, v)\, d\tau. \qquad (10)$$

Because $a\,(\mu, v)$ are known from the current state, it remains to determine $P_0(t + \tau \mid t)$, the probability distribution density for the imminent quiescence time. To calculate this quantity, consider a system in some state $\mathbf{x} = \{X_1, X_2, \ldots X_M\}$, at time t. According to Eqs. (7) and (8), the probability $P_0(t + \delta\tau \mid t)$ that the system remains in the state $\mathbf{x}$ during the small time interval $[t, t + \delta\tau)$ is exactly

$$P_0(t + \delta\tau \mid t) = P_0(t + 0 \mid t)\left(1 - \sum_{\mu=1}^{M} \alpha_\mu \delta\tau + O\,(\delta\tau)\right), \qquad (11)$$

where the quantities α_μ are given by

$$\alpha_\mu = \sum_{\nu=1}^{\mu} a(\mu, \nu) \tag{12}$$

such that the sum in Eq. (11) reflects all possible transitions from the state **x**. By transposition of $P_0(t + 0 \mid t)$ from the left hand side of Eq. (11), division by $\delta\tau$, and taking the limit $\delta\tau \to 0$, a differential equation is obtained for $P_0(t + \tau \mid t)$,

$$\frac{d}{d\tau} P_0(t + \tau \mid t) = -\alpha P_0(t + \tau \mid t), \tag{13}$$

where α is given by

$$\alpha = \sum_{\mu=1}^{M} \alpha_\mu \tag{14}$$

and the initial condition is $\lim_{\tau \to 0} P_0(t + \tau \mid t) = 1$. Equation (13) is a first-order differential equation and may be solved exactly for any time-dependent form of the transition probabilities $\{C(\mathbf{u}_\mu, \mathbf{u}_\nu)\}$. In the special (and typical) case where $C(\mathbf{u}_\mu, \mathbf{u}_\nu)$ is not time dependent, the quiescence time is distributed exponentially [7]:

$$P_0(t + \tau \mid t) = \exp(-\alpha\tau). \tag{15}$$

However, if the system volume V or kernel $K(\mathbf{u}_\mu, \mathbf{u}_\nu)$ are explicitly functions of time, the functional form of $P_0(t + \tau \mid t)$ will differ. In conclusion, the aggregation probability density function for time-independent kernels may be written as

$$P(\mu, \nu; \tau)\, d\tau = a(\mu, \nu) \exp(-\alpha\tau). \tag{16}$$

We now proceed to develop the basic equations for use as selection rules in our MC algorithm. To begin, we note that MC simulation methods are based upon random sampling of probability distributions. For univariate distributions, MC sampling often entails equating a cumulative probability distribution with a random number $r \in [0, 1]$ in order to specify a value of the random variable as an outcome of a random experiment. In our case, we recondition Eq. (16) to permit independent selection of the quiescence time and the imminently aggregating species. An efficient conditioning for this type of distribution is [7]

$$P(\mu, \nu; \tau)\, d\tau = P_2(\mu, \nu \mid \tau) P_1(\tau)\, d\tau, \tag{17}$$

where the probability that the quiescence time is greater than τ is

$$P_1(\tau)\, d\tau = \alpha \exp(-\alpha\tau)\, d\tau, \tag{18}$$

and the probability that the species involved in the imminent aggregation event are at least μ and ν is

$$P_2(\mu, \nu \mid \tau) = \frac{a(\mu, \nu)}{\alpha}. \tag{19}$$

Sampling Eqs. (18) and (19) by MC, the random variables τ, μ, and ν may be specified by the formulas

$$\tau = \frac{1}{\alpha} \ln \left(\frac{1}{r_1} \right), \tag{20}$$

$$\sum_{i=1}^{\mu-1} \sum_{j=1}^{\nu-1} a(i, j) \leq r_2 \alpha < \sum_{i=1}^{\mu} \sum_{j=1}^{\nu} a(i, j), \tag{21}$$

where the numbers r_1 and r_2 ($r_1, r_2 \in [0, 1]$) must be provided by a uniform random number generator. The use of Eqs. (20) and (21) to select the quiescence time and imminently aggregating species forms the basis of our MC algorithm.

3. SIMULATION ALGORITHM

Implementation of the probabilistic description of the aggregation process given in the preceding section requires additional consideration of both the definition of the initial species and the numerical details of computation of the random variables τ, μ, and ν. In this section, we address both issues in greater detail.

3.1. Specification of the Initial State

In real aggregation and polymerization processes, there exist a finite set of particles of composition $\mathbf{u}_i$ ($i \in [1, N]$), as defined in the previous section. Hence, the generalized concentration density $\hat{c}(\mathbf{u}, t)$ possesses the following mathematical form [20]:

$$\hat{c}(\mathbf{u}, t) = \sum_{i=1}^{N} \delta(\mathbf{u} - \mathbf{u}_i). \tag{22}$$

Here $\delta(\mathbf{x})$ is a vector form of Dirac's delta function, such that $f(\mathbf{0}) = \int f(\mathbf{x}) \delta(\mathbf{x}) \, d\mathbf{x}$. "Discrete" aggregation processes such as chemical polymerization explicitly use discontinuous concentration densities such as Eq. (22). For instance, a two-component aggregation process beginning with two types of particles of compositions $\mathbf{u}_1 = (u_0, 0)$ and $\mathbf{u}_2 = (0, v_0)$ at concentrations c_1 and c_2 has the initial concentration density

$$\hat{c}(u, v; 0) = \frac{1}{u_0 v_0} \left(c_1 \delta \left(\frac{u}{u_0} - 1 \right) \delta \left(\frac{v}{v_0} \right) + c_2 \delta \left(\frac{u}{u_0} \right) \delta \left(\frac{v}{v_0} - 1 \right) \right). \tag{23}$$

Due to the discontinuities in Eq. (23) and the fact that all aggregates must be composed of integral amounts of each type of initial particle, the size space $\{u, v\} \in \mathbb{R}^2$ is reduced to a subspace on $\mathbb{N}^2$. That is, every aggregate of composition (u, v) can be thought of as an m, n-mer, since $u = u_0 m$ and $v = v_0 n$. In the context of PBEs, solution of Eq. (2) with the initial condition given by Eq. (23) is equivalent to solution of Eq. (1) with $c(m, n; 0) = c_1 \delta_{m,1} + c_2 \delta_{1,n}$. Likewise, all concentration densities $\hat{c}(\mathbf{u}, 0)$ representing a set of $\mathbf{n}$-mers ($\mathbf{n} = (n_1, n_2, \ldots n_\kappa) \in \mathbb{N}^\kappa$ will result in $\mathbf{n}$-mer aggregates on the same composition space $\mathbb{N}^\kappa$.

Consequently, specification of the initial state of a simulation of a "discrete" process requires only that one define the populations of the species according to $c(\mathbf{n}, t)$. This

process may be done as follows. The system volume V is defined by

$$V = \frac{X_0}{G(\mathbf{u} = \infty, 0)}, \tag{24}$$

where $G(\mathbf{u} = \infty, 0)$ is the total concentration of particles in the initial system and X_0 the total number of particles. Here, care must be taken to ensure that X_0 is large enough to ensure that most species defined by $c(\mathbf{n}, 0)$ are sufficiently populated. Subsequently, X_0 particles must be selected from the initial concentration density $c(\mathbf{n}, 0)$ using the inequality

$$\sum_{i_1=1}^{n_{1,j}-1} \sum_{i_2=1}^{n_{2,j}-1} \cdots \sum_{i_\kappa=1}^{n_{\kappa,j}-1} c(\mathbf{i}, t) \leq r_j G(\mathbf{u} = \infty, 0) < \sum_{i_1=1}^{n_{1,j}} \sum_{i_2=1}^{n_{2,j}} \cdots \sum_{i_\kappa=1}^{n_{\kappa,j}} c(\mathbf{i}, t), \tag{25}$$

where r_j is a uniform random number on the interval $[0, 1)$ for the specification of the jth ($j \in [1, X_0]$) particle such that $\mathbf{n}_j = (n_{1,j}, n_{2,j} \ldots n_{\kappa,j})$. The similarity of Eqs. (25) and (21) is a consequence of the fact that both are MC-selection rules for discrete variables, summing discrete distribution densities until excess of a random number. Given these X_0 particles, the initial species $\mu \in [1, M]$ are defined as particles with common compositions $\mathbf{n}_\mu$. The populations of these species X_μ are equal to the numbers of particles chosen by Eq. (25) with composition $\mathbf{n}_\mu$.

While the preceding discussion of the initial species has focused on the definition of species in a "discrete" process, the procedure may be extended to aggregation processes featuring particles of arbitrary size. The deterministic approach to this problem is represented by Eq. (2), where the concentration density used to characterize the state of a two-component aggregation process is usually considered to be a *continuous* function on $(u, v) \in \mathbb{R}^2$. Strictly speaking, this is an approximation of the microphysically exact Eq. (22), as continuity of $\hat{c}(\mathbf{u}, t)$ implies that the concentration of particles of a specific composition $\mathbf{u}$ is zero. Hence, because individual species are not explicitly specified by a continuous $\hat{c}(\mathbf{u}, 0)$, it suffices to define them such that their cumulative distribution is equal to that of $\hat{c}(\mathbf{u}, 0)$,

$$G(\mathbf{u}, t) = \int_0^{\mathbf{u}} \hat{c}(\mathbf{u}, t) \, d\mathbf{u}$$
$$= \sum_{\mu=1}^{M} X_\mu \theta(\mathbf{u} - \mathbf{u}_\mu), \tag{26}$$

where $\theta(\mathbf{x})$ is a vector form of Heaviside's unit step function, defined by

$$\theta(\mathbf{x}) = \prod_{i=1}^{\kappa} \theta(x_i) \tag{27}$$

such that $\theta(\mathbf{x}) = \int_0^{\mathbf{u}} \delta(\mathbf{x}) \, d\mathbf{x}$. Although expressed in terms of species instead of particles, Eq. (26) is a direct result of Eq. (22). Consequently, it is exact for both the initial and all subsequent states, provided that the initial species are defined in accordance with $\hat{c}(\mathbf{u}, 0)$.

Like discrete processes, the generation of initial species for continuous processes begins with the definition of the system volume using Eq. (24) and subsequent generation of X_0 particles by MC. Due to the fact that the compositions are continuous variables in this case

$(\mathbf{u}_j \in \mathbb{R}^{\kappa})$, their generation requires integration over $u_{1,j}$, $u_{2,j}$, and so forth, until a random number is exceeded. Symbolically, we represent this as

$$r_j G(\mathbf{u} = \infty, t) = \int_0^{\mathbf{u}_j} \hat{c}(\mathbf{u}, t)\, d\mathbf{u}. \tag{28}$$

Because Eq. (28) is an exact MC-selection formula, the cumulative composition distribution of the resulting particles will equal $G(\mathbf{u}, 0) = \int_0^{\mathbf{u}} \hat{c}(\mathbf{u}, 0)\, d\mathbf{u}$ to the extent that a continuous form of $\hat{c}(\mathbf{u}, 0)$ can approximate the concentration density for a finite set of particles.

As in the discrete case, the initial species are defined using these X_0 MC-generated particles. However, the method employed for discrete processes is not the most efficient in this case, as each particle composition chosen by Eq. (28) will be unique. As a result, X_0 species would result, with little chance that any combination of these species would ever produce a species with a population greater than unity during the following simulation process. Thus, while theoretically satisfactory, direct use of compositions chosen by Eq. (28) to define initial species is numerically inefficient.

A more efficient way to define the initial species is possible by discretizing the initial composition space into component "bins." So long as these species obey Eq. (26), they are as satisfactory as the aforementioned random set of species potentially specified by Eq. (28). In the following implementation, we employ linear discretization of the composition space, which transforms the continuous composition space into an effectively discrete one, minimizing the combinatorial complexity of the composition spaces into their aggregates and, thus, the number of species.

In order to illustrate the method, we consider here a two-component aggregation process with an initial concentration density $\hat{c}(\mathbf{u}, 0)$ on a continuous composition space. This space may be discretized by subdividing $\mathbf{u} = (u_1, u_2)$ into $\mathcal{M}_1 \times \mathcal{M}_2$ intervals with abscissas

$$w_1(k_1) = \frac{2k_1 + 1}{2\mathcal{M}_1 + 1} w_1(\mathcal{M}_1) \quad k_1 \in [1, \mathcal{M}_1] \subset \mathbb{N} \tag{29}$$

and

$$w_2(k_2) = \frac{2k_1 + 1}{2\mathcal{M}_1 + 1} w_2(\mathcal{M}_2) \quad k_2 \in [1, \mathcal{M}_2] \subset \mathbb{N}, \tag{30}$$

where $w_1(\mathcal{M}_1) = \max(u_{1,j})$ and $w_2(\mathcal{M}_2) = \max(u_{2,j})$ are the maximum amounts of the two components in any of the X_0 initial particles. Each species μ with composition $\mathbf{u}_\mu = (u_{1,\mu}, u_{2,\mu})$ is defined by a unique set of composition intervals (k_1, k_2) such that

$$u_{1,\mu} = \frac{1}{2}(w_1(k_1 - 1) + w_1(k_1)), \tag{31}$$

$$u_{2,\mu} = \frac{1}{2}(w_2(k_2 - 1) + w_2(k_2)), \tag{32}$$

and

$$X_\mu = \int_{\mathbf{w}(k_1 - 1, k_2 - 1)}^{\mathbf{w}(k_1, k_2)} \hat{c}(\mathbf{u}, t)\, d\mathbf{u}$$

$$= \sum_{j=1}^{X_0} [\theta(\mathbf{w}(k_1, k_2) - \mathbf{u}_j) - \theta(\mathbf{w}(k_1 - 1, k_2 - 1) - \mathbf{u}_j)], \tag{33}$$

where $\mathbf{w}(k_1, k_2) = (w_1(k_1), w_2(k_2))$. In summary, Eqs. (31) and (32) ascribe a single composition to the X_μ particles defined by Eq. (28) that fall in the composition range $\{[w_1(k_1 - 1), w_2(k_2 - 1)], [w_1(k_1), w_2(k_2)]\}$. Although this example addresses the definitions of initial species in a two-component process, the extension of Eqs. (30), (32), and (33) to systems with more than two components is direct.
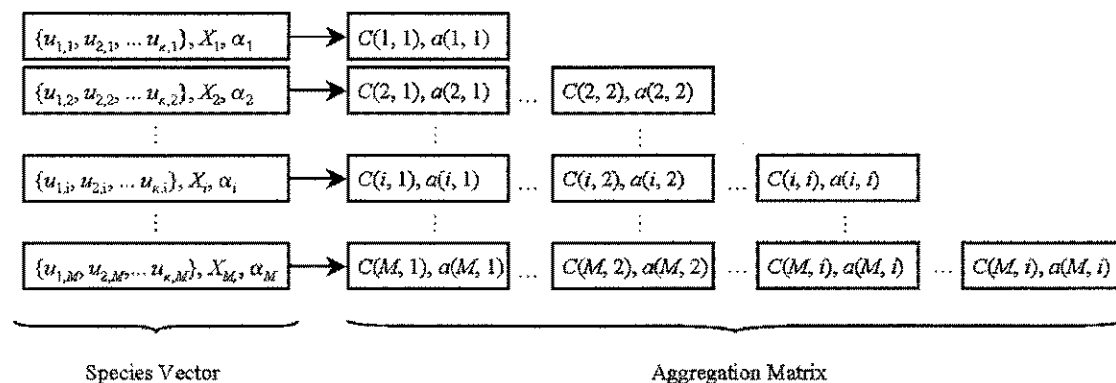
3.2. Aggregation Table

Given an initial state, the process of simulating its time evolution follows directly from Eqs. (20) and (21) in the previous section. The MC simulation algorithm goes as follows.

(i) Compute α (14).

(ii) Choose a quiescence time and the species involved in the subsequent event according to Eqs. (20) and (21).

(iii) Update the populations of the reactant and product species, and increment the time by τ.

(iv) Update all $a(i, j)$ affected by the change of those populations.

(v) Repeat.

For processes with time-independent kernels, the computationally intensive steps are (i), (ii), and (iv), potentially requiring $O(M^2)$, $O(M^2)$, and $O(M)$ additions, respectively. Furthermore, upon generation of a new species, $M + 1$ new transition probabilities must be created and stored for aggregation events with preexisting species, involving the computation of $M + 1$ kernels. As M becomes large, the accounting after an aggregation event is the rate-limiting step of the algorithm. However, the postaggregation processing can be handled very simply and efficiently using an aggregation table (Fig. 1).

The aggregation table organizes the aggregation and species data in a way that allows fast and efficient implementation of every step in the simulation procedure. The table consists of a species vector specifying the state of the system and a corresponding sparse "aggregation matrix" containing the transition probabilities from the state specified by the species vector. The μth element of the species vector holds the composition $\mathbf{u}_\mu$, the population X_μ, and the partial sum α_μ for the μth species. Likewise, the μth row of the aggregation matrix holds the values of $C(\mu, \nu)$ and $a(\mu, \nu)$ for the events between species μ and all species $\nu \in [1, \mu]$. The order of the species in the species vector is determined by their birth and death.

Species Vector   Aggregation Matrix

FIG. 1. Structure of the aggregation table. Each species i in the species vector has $\{u_{1,i}, u_{2,i}, \ldots u_{\kappa,i}\}$ as its composition, X_i as its population, and α_i as the sum of all $a(i, j)$ ($j \in [1, i]$) in the corresponding row in the aggregation matrix.

The use of partial sums $\{\alpha_\mu\}$ confers dramatic improvements in efficiency in the computation of steps (i) and (ii) over the uses of Eqs. (20)–(21) alone. Because α may be computed using Eq. (14), step (i) can be executed with only $O(M)$ additions. Furthermore, the partial sums simplify selection of the imminently aggregating species: instead of subtracting each $a(\mu, \nu)$ from the quantity $r_2\alpha$ in Eq. (21), one may subtract each α_i from $r_2\alpha$ until the result is negative. That is, the index of the first aggregating species is the lowest integer μ for which

$$r_2\alpha - \sum_{i=1}^{\mu} \alpha_i < 0. \tag{34}$$

Subsequently, the index of the second aggregating species is the lowest integer ν for which

$$r_2\alpha - \sum_{i=1}^{\mu} \alpha_i - \sum_{j=1}^{\nu} a(\mu, j) < 0. \tag{35}$$

Hence, the number of operations in the aggregation selection process is reduced from $O(M^2)$ to $O(M)$. Graphically, the choice is made by scanning down the partial sums in the table until the μth row, and then the transition probabilities across the matrix to the νth column. We note that although Gillespie implemented the stochastic approach in a significantly different way, his full conditioning method [6] employs a similarly judicious use of partial sums to reduce the number of computations involved in species selection from $O(N^2)$ to $O(N)$ when the system has N particles.

After identification of the "reactant" species, the aggregation table permits a simple means of updating their populations and aggregation information. Here, only the μth and νth rows of the species vector require population readjustment. Furthermore, step (iv) only requires updating of the μth and νth rows and columns of the aggregation matrix according to Eqs. (7) and (8). As these rows are updated, the partial sums α_μ, α_ν, and α_π may be updated concurrently. Thus, the structure of the table obviates the need for a dependency graph to determine which transition probabilities are affected by the immediate event.

Subsequently, the identification or creation of the product species π must be addressed. In the deterministic formalism, the relationships between all potential reactant and product species are implicitly defined through the PBE. As a result, discretization of the composition space in PBEs such as Eq. (2) in the course of numerical integration has the potential to violate the underlying conservation laws implied by the exact PBE [10, 13, 14]. For instance, a discretized PBE might imply that two species defined by masses m_1 and m_2 would aggregate to form a species m_4, where $m_4 \neq m_1 + m_2$. In contrast, our simulation method employs microscopic conservtion of properties or components, allowing it to avoid these discretization problems. If species are defined by conserved quantities such as the number of monomers or mass of each component, then product species may be defined by an equation such as $\mathbf{u}_\pi = \mathbf{u}_\mu + \mathbf{u}_\nu$. Furthermore, if some of the properties stored in $\mathbf{u}$ are not conserved, such as surface area in droplet coalescence, they may be computed directly and exactly, given the pertinent physical laws pertaining to their definition. Hence, our simulation algorithm addresses the definition of the properties of product species in an exact and general way, enforcing conservation laws on an event-by-event basis.

The aggregation table may also be used to simplify the bookkeeping associated with the product species π. To begin, the species vector must be searched in order to determine whether or not there exists a species with composition $\mathbf{u}_\pi$, requiring at most M Boolean operations—insignificant in comparison with the floating point operations involved with

the rest of the algorithm. If found in the species vector, the population of species π must be incremented and the πth row and column of the aggregation matrix must be updated. If no species with composition $\mathbf{u}_\pi$ can be found, the species vector is extended to accomodate a new species with composition $\mathbf{u}_M = \mathbf{u}_\pi$ and population $X_M = 1$, along with a corresponding row of the aggregation matrix.

Depopulated species may be removed from the aggregation table just as easily and efficiently as new species are added. On complete consumption of some species μ, the μth entry in the species vector and the μth row and column from the aggregation matrix may be deleted and their memory locations deallocated without any copying of information or disturbance of the rest of the table. This process is easily handled by dynamic allocation of memory and the use of pointers to construct the aggregation table. In practice, we have found the object-oriented architectures supported by C++ particularly helpful in our implementation. Figure 2 outlines the processes of addition, removal, and updating of aggregation events affected by the latest event.

Lastly, if the kernel $K(\mathbf{u}_\mu, \mathbf{u}_\nu)$ is a function of time, every $C(\mathbf{u}_\mu, \mathbf{u}_\nu)$ and $a(\mu, \nu)$ may need to be updated after each event. Consequently, steps (i) and (iv) will require $O(M^2)$ operations. However, step (ii) remains an $O(M)$ operation, since the kernels are already updated from the preceding loop. While more computationally demanding, the relative improvement over particle accounting algorithms increases significantly in this case, as these become $O(N^2)$ in this limit. For large initial numbers of particles, the difference
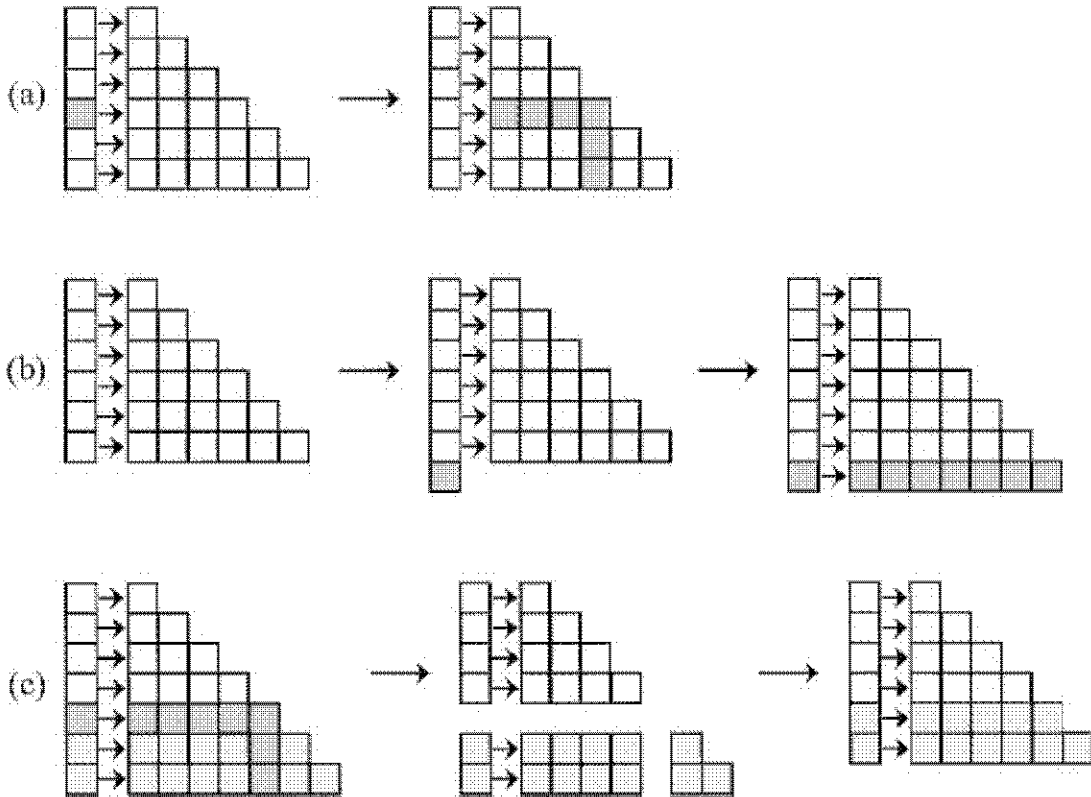
FIG. 2. Maintenance of the aggregation table. (a) When the population of species i is changed in the species vector, only the ith and jth columns in the aggregation matrix must be updated. (b) If a new species is produced, it is added to the end of the species vector and its aggregations are placed in a new row at the bottom of the aggregation matrix. (c) If the ith species is completely consumed, its entry in the species vector is deleted, as are the ith rows and columns in the aggregation matrix. Subsequently, the table may be condensed and the empty entries deallocated without affecting the other entries in the table.

in execution speed is remarkable. In the special cases where all of the kernels have the same time dependence or the volume is a function of time, the selection criterion Eq. (19) will be unaffected outright. In this case, the aggregation table need only contain the time-independent parts of the kernels and partial sums $\{\alpha_\mu\}$. Although Eq. (16) will not result in an exponential distribution in these cases, the simulations of processes with these kernels will exhibit the same efficiency as those with time-independent kernels (or volume).

3.3. Computational Efficiency

In the preceding discussion, we have shown that our species accounting algorithm requires $O(M)$ operations per time step, whereas particle accounting algorithms require $O(N)$ operations, where N is the number of particles in the simulation. Furthermore, we have shown that species accounting reduces the storage requirements from $O(N^2)$ to $O(M^2)$. In order to more quantitatively compare the performance of these two approaches to MC simulation, we now address the relationship between the number of species M and number of particles N in a more quantitative way.

Although the exact relationship between N and M depends on the process, the maximum number of species $M_{\max}$ can be related to the total number of constituent particles (or monomers) by consideration of monomer conservation. Consider an aggregation process in which there are Ω_k monomers of the kth component in the system ($k \in [1, \kappa]$). A detailed balance on each component gives

$$\Omega_1 = \sum_{n_1=0}^{\omega_1} n_1 \sum_{n_2=0}^{\omega_2} \sum_{n_3=0}^{\omega_3} \cdots \sum_{n_\kappa=0}^{\omega_\kappa} X(n_1, n_2, \ldots n_\kappa)$$

$$\Omega_2 = \sum_{n_1=0}^{\omega_1} \sum_{n_2=0}^{\omega_2} n_2 \sum_{n_3=0}^{\omega_3} \cdots \sum_{n_\kappa=0}^{\omega_\kappa} X(n_1, n_2, \ldots n_\kappa)$$

$$\vdots$$

$$\Omega_\kappa = \sum_{n_1=0}^{\omega_1} \sum_{n_2=0}^{\omega_2} \sum_{n_3=0}^{\omega_3} \cdots \sum_{n_\kappa=0}^{\omega_\kappa} n_\kappa X(n_1, n_2, \ldots n_\kappa),$$

(36)

where ω_k is the largest amount of the kth component in any species. While most of the species in the above sums will have population zero in practice, let us consider the case where each is singly populated, maximizing the number of potential species. In this case, Eqs. (36) become

$$\Omega_1 = \frac{1}{2}\omega_1(\omega_1 + 1)\prod_{k=2}^{\kappa}(\omega_k + 1) \sim \frac{1}{2}(\omega_1 + 1)\prod_{k=1}^{\kappa}(\omega_k + 1)$$

$$\Omega_2 = \frac{1}{2}\omega_2(\omega_2 + 1)\prod_{k=1,k\neq 2}^{\kappa}(\omega_k + 1) \sim \frac{1}{2}(\omega_2 + 1)\prod_{k=1}^{\kappa}(\omega_k + 1)$$

$$\vdots$$

(37)

$$\Omega_\kappa = \frac{1}{2}\omega_\kappa(\omega_\kappa + 1)\prod_{k=1}^{\kappa-1}(\omega_k + 1) \sim \frac{1}{2}(\omega_\kappa + 1)\prod_{k=1}^{\kappa}(\omega_k + 1).$$

Because the maximum number of species is equal to the number of possible compositions $\mathbf{n} = (n_1, n_2, \ldots n_\kappa)$ (with the exception of $\mathbf{n} = \mathbf{0}$), $M_{\max}$ may be written in terms of $\{\omega_k\}$

$$M_{\max} = \left(\sum_{n_1=0}^{\omega_1} \sum_{n_2=0}^{\omega_2} \cdots \sum_{n_\kappa=0}^{\omega_\kappa} 1 \right) - 1 \simeq \prod_{k=1}^{\kappa} (\omega_i + 1). \tag{38}$$

Finally, combination of Eqs. (37) and (38) gives the relationship between $M_{\max}$ and the number of particles of each component $\{\Omega_k\}$:

$$\prod_{i=1}^{\kappa} \Omega_i \sim 2^{-\kappa} \prod_{i=1}^{\kappa} (\omega_i + 1) \left(\prod_{i=1}^{\kappa} (\omega_i + 1) \right)^{\kappa}$$

$$= 2^{-\kappa} \left(\prod_{i=1}^{\kappa} (\omega_i + 1) \right)^{\kappa+1}$$

$$= 2^{-\kappa} M_{\max}^{\kappa+1}. \tag{39}$$

Equation (39) gives the relationship between the maximum number of particles and the maximum number of species. While a multicomponent particle accounting algorithm would have at most $N_{\max} = \Omega_1 + \Omega_2 + \ldots \Omega_\kappa$ operations per time step, our algorithm requires only $O(M_{\max}) = O((\Omega_1 \Omega_2 \ldots \Omega_\kappa)^{1/(\kappa+1)})$. For single-component aggregation processes ($\kappa = 1$), this reduces to $O(N_{\max}^{1/2})$—the same as the optimized single-component MC simulation algorithms of Spouge [26] and Thorn et al. [30].

As indicated by Eq. (39), species accounting dramatically reduces both computer storage and simulation time. For example, a simulation of 50,000 initial particles evenly distributed into two types will require memory for about 10^9 kernels and 50,000 particles in the state vector and their properties, while a species accounting approach will only require memory for at most ~3400 species and ~10^7 kernels and transition probability densities $a(\mathbf{u}_\mu, \mathbf{u}_\nu)$. In practice, the maximum number of species in a simulation is typically much less than that given by Eq. (39), such that the computational constraints of our species accounting implementation are significantly smaller still. However, it should be noted that with each additional component, the number of ways of creating new species increases geometrically. Just as molecules deplete a point in space by diffusion much faster in three dimensions than in two or one dimensions, particles deplete their initial distribution much faster in a multi-component aggregation than in a single-component aggregation. Consequently, continuous multicomponent aggregation simulations based on our algorithm tend to the particle accounting limit as complete aggregation is approached. When simulating tens of thousands of particles of multiple components, one must ensure sufficient memory for storage of potentially hundreds to thousands of species and their millions of aggregation kernels.

4. ILLUSTRATIVE EXAMPLES

In order to demonstrate the feasibility and robustness of the algorithm, we now present some results of MC simulations of two-component processes for a few representative kernels. In the course of illustrating the algorithm's implementation, our results also explicitly demonstrate the differences between the stochastic and deterministic approaches to aggregation kinetics. We begin by considering three classes of kernels that permit analytical solution

of Eq. (1). Subsequently, we present numerical results for two continuous two-component aggregation processes.

4.1. Discrete Processes

In order to represent some representative mathematical behaviors exhibited by aggregation kernels, let us consider the three two-component aggregation kernels:

$$K(m, n \mid m', n') = \beta \quad \beta = \text{const}, \tag{40}$$

$$K(m, n \mid m', n') = B(m + n + m' + n') \quad B = \text{const}, \tag{41}$$

and

$$K(m, n \mid m', n') = b(m + n)(m' + n') \quad b = \text{const}. \tag{42}$$

Defining an index of homogeneity λ by the formula

$$K(su, sv \mid su', sv') = s^\lambda K(u, v \mid u', v'), \tag{43}$$

these kernels represent processes with progressively increasing degrees of dependence on the compositions of the aggregating particles. The first of these is insentivive ($\lambda = 0$), the second is intermediate ($\lambda = 1$), and the third possesses the strongest composition dependence ($\lambda = 2$). For each homogeneity index, unique behaviors are observed in both the deterministic and stochastic approaches to aggregation kinetics. Moreover, simulation of processes with these kernels permits a direct comparison between the two approaches. Lushnikov has shown that if a two-component kernel is dependent only on the total numbers of monomers in each "reacting" aggregate

$$K(m, n \mid m', n') = K(m + n, m' + n') \tag{44}$$

and the initial state of the system features monomers only, as in Eq. (23), then the composition distribution may be expressed as [16]

$$c(m, n; t) = \binom{m}{n} \left(\frac{c_1}{c_0}\right)^m \left(\frac{c_2}{c_0}\right)^n c(m + n, t) \quad c_0 = c_1 + c_2. \tag{45}$$

In Eq. (45), $c(m + n, t)$ is the concentration of particles composed of $(m + n)$ monomers of either type. It may be determined by solution of Smoluchowski's equation [25],

$$\frac{\partial c(i, t)}{\partial t} = \frac{1}{2} \sum_{j=1}^{i-1} K(j, i - j)c(j, t)c(i - j, t) - \sum_{j=1}^{\infty} K(i, j)c(i, t)c(j, t), \tag{46}$$

using the initial condition $c(i, 0) = c_0 \delta_{i,1}$, where $K(i, j)$ is the form of the kernel on the right hand side of Eq. (44). Like Eqs. (1) and (2), Smoluchowski's has few analytical solutions. However, given the initial condition $c(i, 0) = c_0 \delta_{i,1}$, solutions *are* known for the constant, sum, and product kernels $K(i, j) = \beta$, $B(i + j)$, and $b(i \times j)$ [8, 18, 25]

TABLE I
Analytical Solutions of Smoluchowski's Equation

$K(i, j)$	$c(i, t)$	
β	$4c_0 \dfrac{(T)^{i-1}}{(T+2)^{i+1}}$	$T = \beta c_0 t$
$B(i + j)$	$c_0(1 - \phi)\dfrac{(i\phi)^{i-1}}{\Gamma(i+1)}e^{-i\phi}$	$\phi = 1 - \exp(-Bc_0 t)$
$b(i \times j)$	$\begin{cases} c_0 \dfrac{(iT)^{i-1}}{\Gamma(i+1)}e^{-iT}, & T \leq 1 \\[2ex] \dfrac{c_0}{T}\dfrac{(i)^{i-1}}{\Gamma(i+1)}e^{-i}, & T < 1 \end{cases}$	$T = bc_0 t$

Note. Solutions for initial condition $c(i, 0) = c_0\delta_{i,1}$. Parameters β, B, and b are constants.

(Table I). Consequently, analytical solution of Eq. (1) is possible with the kernels given by Eqs. (40)–(42).

In order to compare the results of our algorithm with these analytical solutions to Eq. (1), simulations of processes with the two-component constant, sum, and product kernels were conducted with $c_1 = 10,000$, $c_2 = 20,000$, and $V = 1$—conditions that sufficiently describe an "infinite" system. In Figs. 3–5 we show results from individual simulation runs along with the analytical size distributions given by Eq. (45) for all three kernels. Despite the fact that PBEs describe the time evolution of the *average* results of the process while MC simulations represent a *single* experiment, the agreement between individual MC-simulation results and analytical solutions of the PBE is excellent, with most of the differences resulting from stochastic fluctuations when $c(m, n; t) \sim O(1/V)$. In accordance with the fact that PBEs describe the average behavior of a process, differences between the averages of several simulations and the analytical solutions of the PBEs were negligible. Consequently, the average MC results predicted $c(m, n; t)$ to a precision greater than V^{-1}. Execution of multiple simulations also provides a means of determining the innate fluctuation of aggregation processes. Just as the average concentration of m, n-mers in solution at time t can be expressed as $c(m, n; t) \simeq \langle X_{m,n} \rangle / V$, so too can other statistics, such as the standard deviation.

In addition to reproducing the composition distributions $c(m, n; t)$, the simulation results also preserved all of their moments, defined by

$$M_{i,j}(t) = \sum_{m=0}^{\infty} \sum_{n=0}^{\infty} m^i n^j c(m, n; t). \tag{47}$$

In Figs. 6–8 we show some of the moments resulting from both the analytical solutions of the PBE and the MC simulation results. In general, the moments of the results of the PBE and MC simulations for the sum and constant kernels agree very well until the physical limit of complete aggregation. However, there are subtle differences in the behaviors of the moments from the deterministic and stochastic approaches in this limit. In real and MC simulated systems, a single particle containing all of the mass of the initial particles is formed in the limit of complete aggregation. At this point, all moments (except $i = j = 0$)
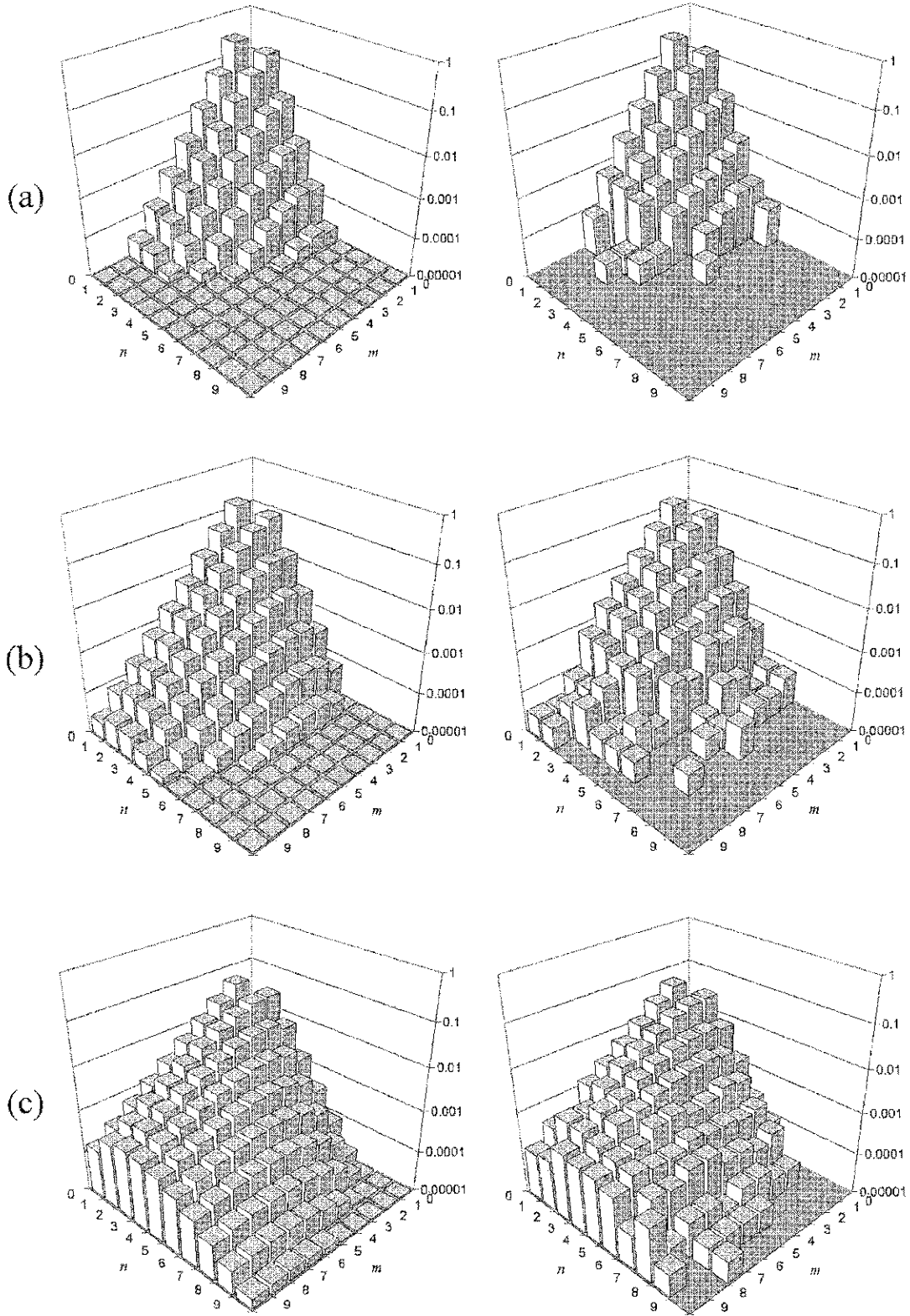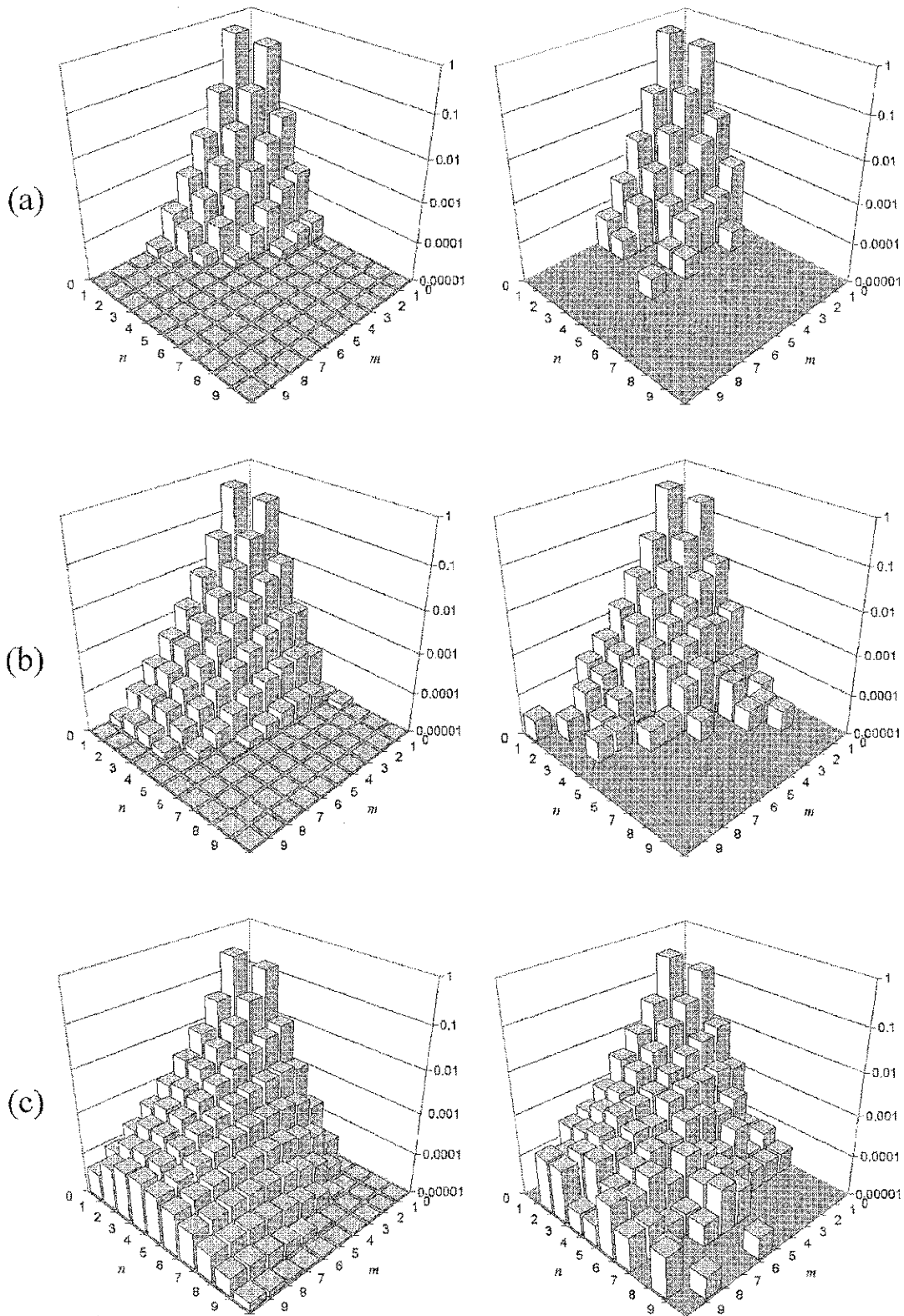
FIG. 3. Normalized discrete particle size distributions $c(m, n; t)/c_0$ resulting from a constant kernel at (a) $T = 1.0$, (b) $T = 2.0$, and (c) $T = 5.0$, where $T = \beta c_0 t$. Distributions from the analytical solution of the PBE are given on the left, and those from MC simulation are given on the right. Simulations were conducted with $c_1 = 10,000$, $c_2 = 20,000$, and $V = \beta = 1.0$.
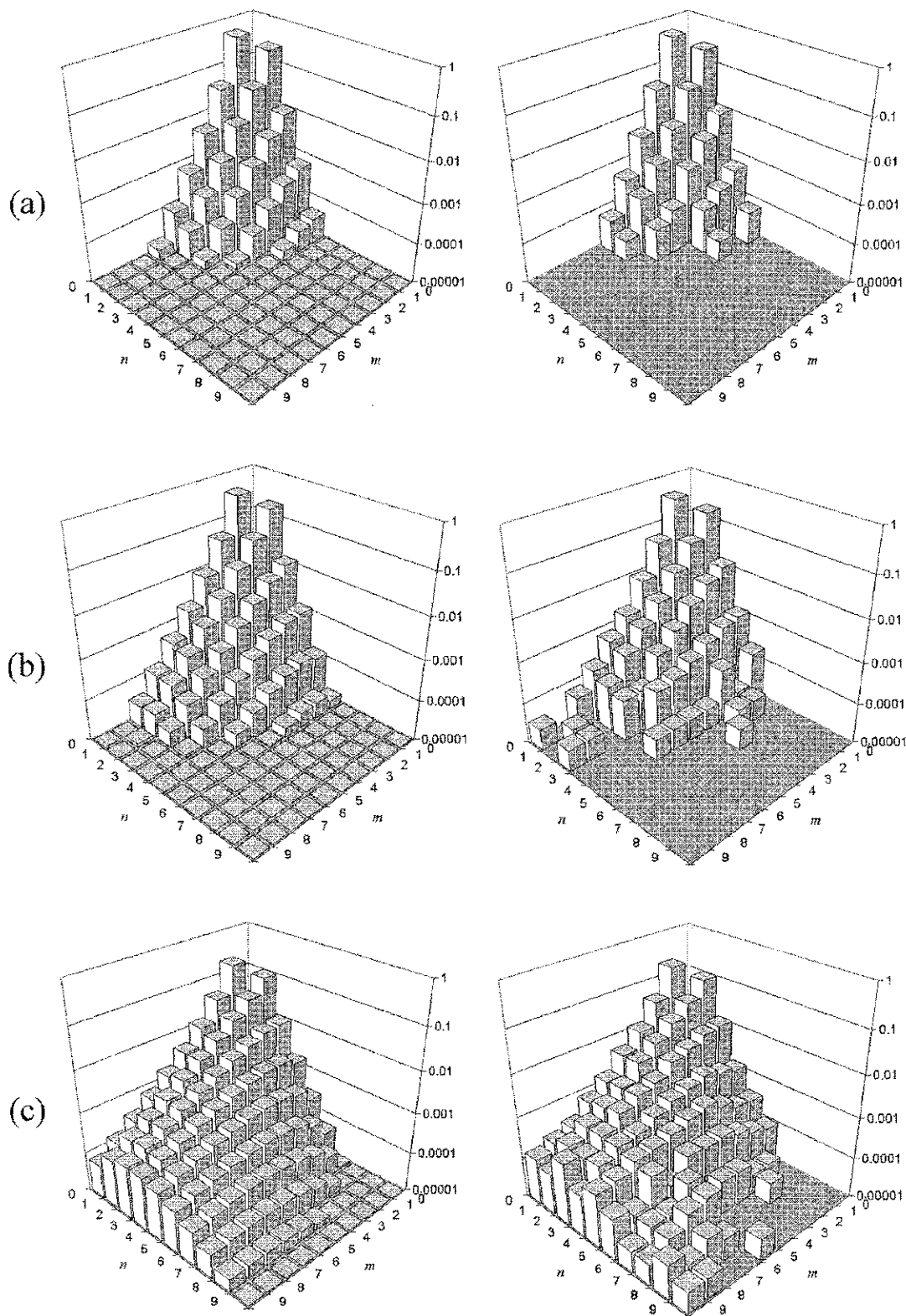
FIG. 4. Normalized discrete particle size distributions $c(m, n; t)/c_0$ resulting from a sum kernel at (a) $\phi = 0.14$, (b) $\phi = 0.24$, and (c) $\phi = 0.5$, where $\phi = 1 - \exp(-Bc_0t)$. Distributions from the analytical solution of the PBE are given on the left, and those from MC simulation are given on the right. Simulations were conducted with $c_1 = 10,000$, $c_2 = 20,000$, and $V = B = 1.0$.

FIG. 5. Normalized discrete particle size distributions $c(m, n; t)/c_0$ resulting from a product kernel at (a) $T = 0.21$, (b) $T = 0.39$, and (c) $T = 0.81$, where $T = bc_0 t$. Distributions from the analytical solution of the PBE are given on the left, and those from MC simulation are given on the right. Simulations were conducted with $c_1 = 10{,}000$, $c_2 = 20{,}000$, and $V = b = 1.0$.
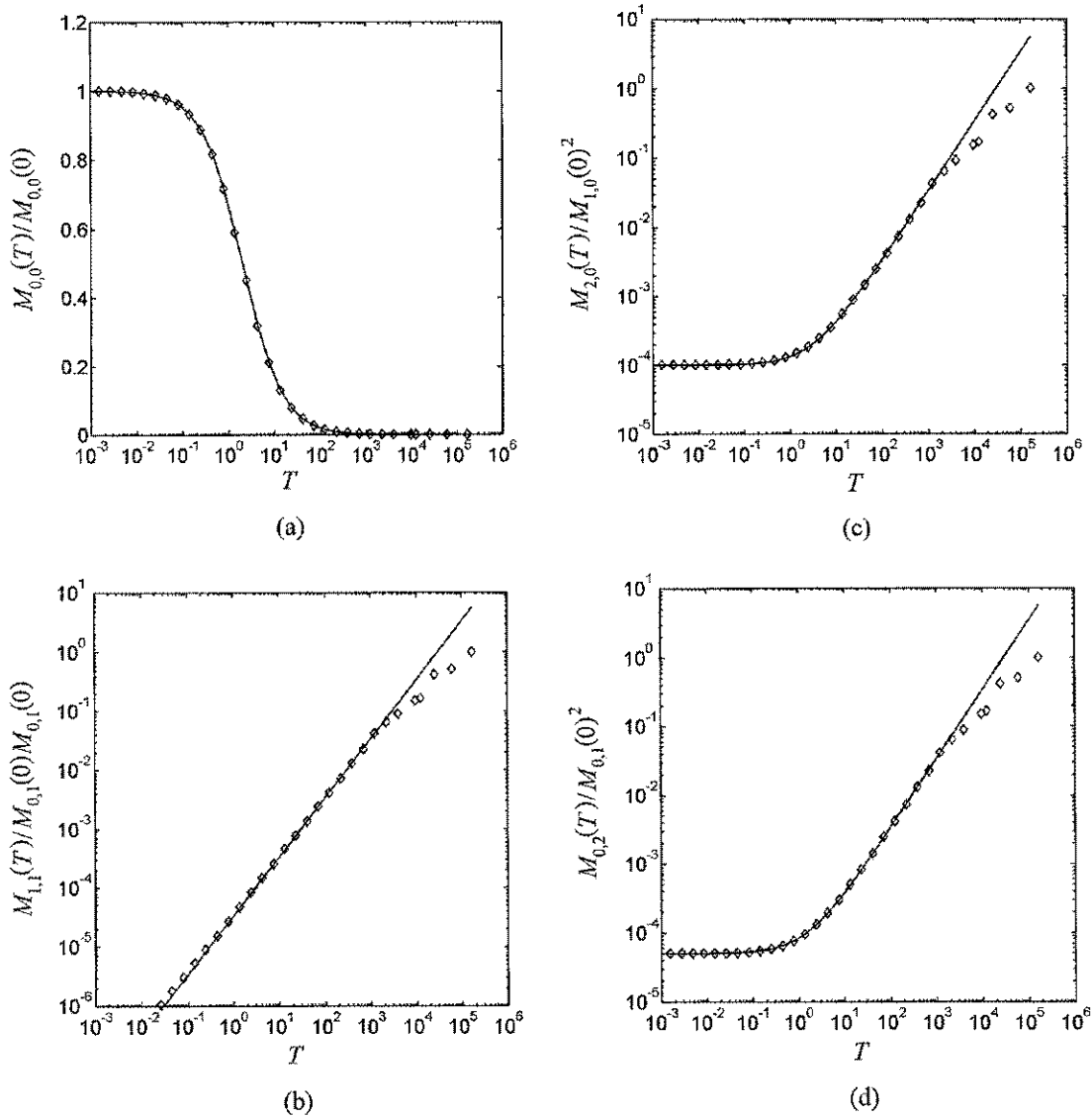
FIG. 6. Normalized zeroth and second moments for the two-component constant kernel. Lines are results from the PBE, and points are results from MC simulation.

exhibit the following limiting behavior:

$$\lim_{t \to \infty} \frac{M_{i,j}(t)}{M_{1,0}^i M_{0,1}^j} = 1; \quad i + j > 0. \tag{48}$$

As shown in Figs. 6–8 and Table II, the moments of the composition distributions originating from the analytical solutions of the PBE do not have the limiting behavior described by Eq. (48), but *exceed* unity at finite times. Moreover, the solution to the PBE with the two-component product kernel features unrealistic behaviors such as failure to conserve mass (Figs. 8b and 8c) and divergence of the second moments (Figs. 8d–8f). The reasons for these behaviors have been detailed elsewhere [2, 5, 6, 16, 20, 21, 28], and result from the fact that deterministic rate laws are valid only for "infinite systems," that is, systems with "large" numbers of particles in "large" volumes. While this thermodynamic limit assumption is sufficient for most kinetic processes, irreversible aggregation and polymerization represent special cases in that they may start large but consume particles until a single
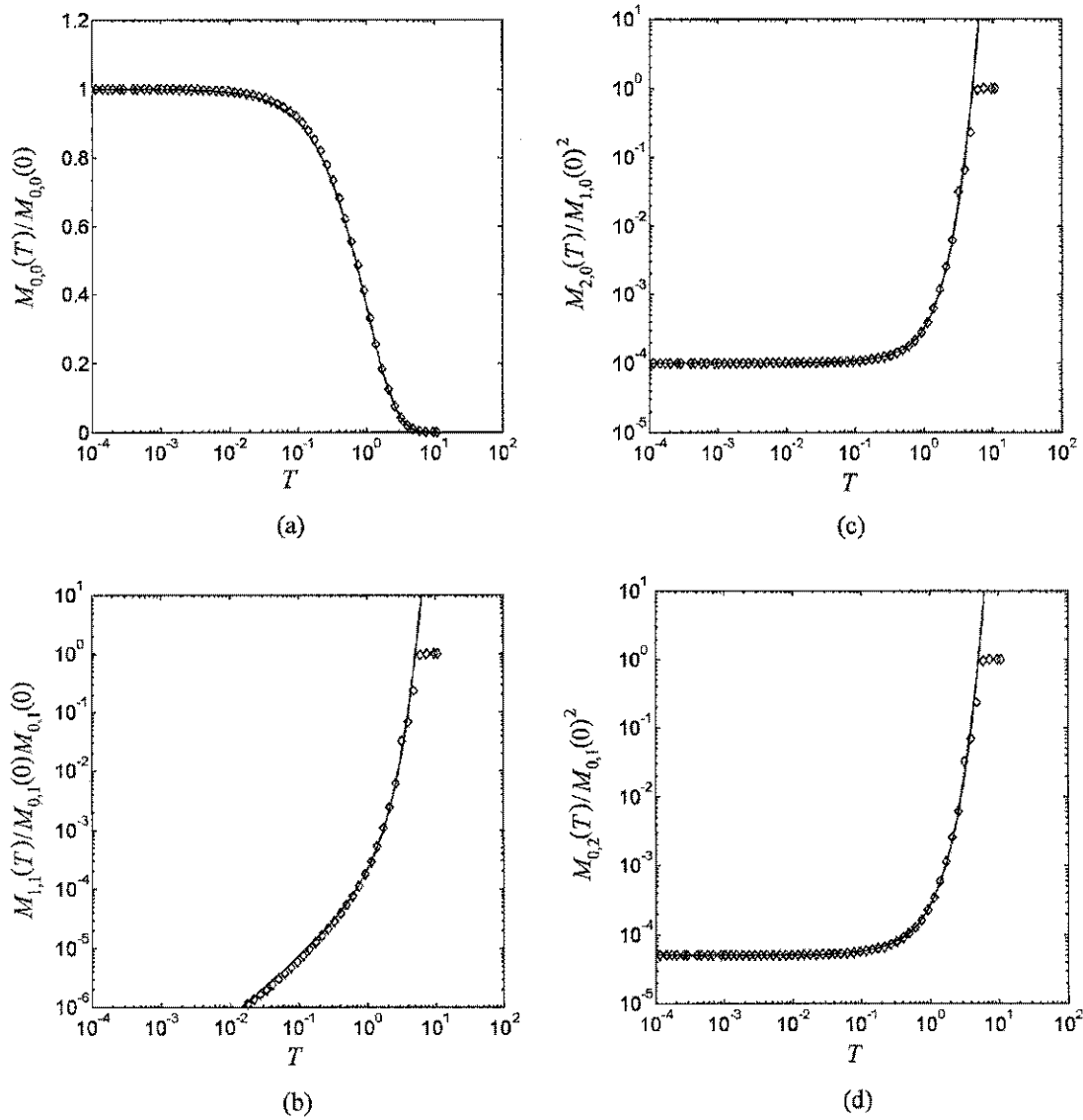
FIG. 7. Normalized zeroth and second moments for the two-component sum kernel. Lines are results from the PBE, and points are results from MC simulation $(T = Bc_0 t)$.

macroparticle remains. Consequently, the neglect of small population corrections in PBEs causes unrealistic behavior as the total population of particles becomes small. Because our MC simulation method exactly employs the stochastic approach without approximation, it can predict the behavior of aggregation processes exactly at *all* times.

In the special case of the product kernel, the moments of the MC and PBE results have significantly different behaviors at the gel transition—a point in the aggregation process at which a "macroscopic" aggregate forms. Ziff's conjecture states that solutions of single-component PBEs with kernels with $\lambda > 1$ and monodisperse initial conditions exhibit the following properties at what is known as the gel point, t_g [33]:

$$M_1(t > t_g) < M_1(0),\tag{49}$$

$$M_i(t \geq t_g) = \infty \quad i = 2, 3, \ldots\tag{50}$$

Equations (49) and (50) represent violation of mass conservation and formation of particles of infinite size, respectively. Mathematically, this behavior results from a divergence of the series defined by Eq. (47), outside of its radius of convergence $[0, t_g]$. For the constant and
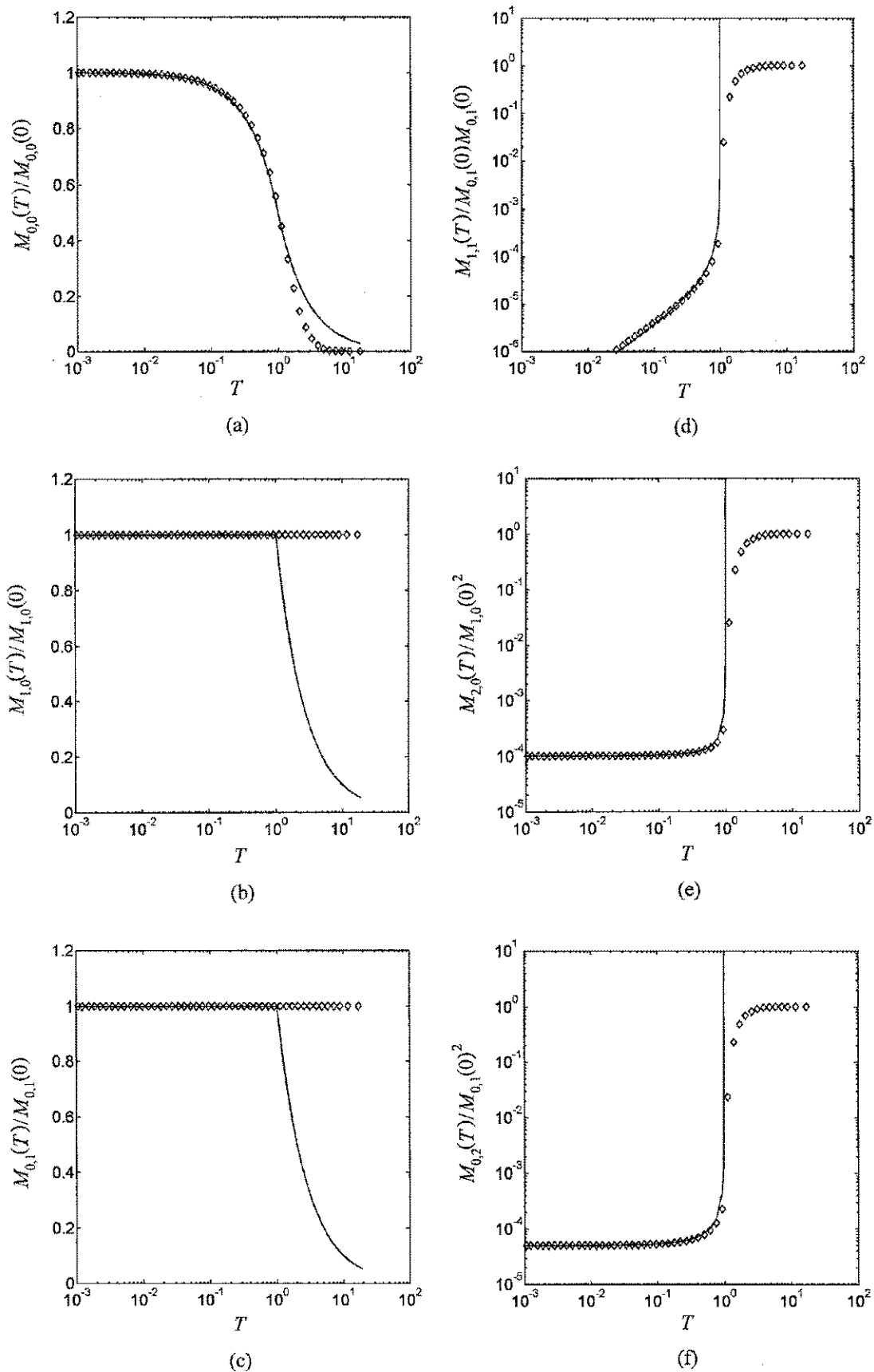
FIG. 8. Normalized zeroth and second moments for the two-component product kernel. Lines are results from the PBE, and points are results from MC simulation.

TABLE II
Moments of the Composition Distributions from Lushnikov's Equation with Two-Component Constant, Sum, and Product Kernels

	Constant kernel	Sum kernel	Product kernel
$M_{0,0}$	$\dfrac{2c_0}{T+2}$	$c_0(1-\phi)$	$\begin{cases} c_0\left(1-\dfrac{1}{2}T\right), & T \le 1 \\[2mm] \dfrac{1}{2}c_0 T, & T > 1 \end{cases}$
$M_{1,0}$	c_1	c_2	$\begin{cases} c_1, & T \le 1 \\[2mm] \dfrac{c_1}{T}, & T > 1 \end{cases}$
$M_{0,1}$	c_1	c_2	$\begin{cases} c_2, & T \le 1 \\[2mm] \dfrac{c_2}{T}, & T > 1 \end{cases}$
$M_{1,1}$	$c_0\dfrac{c_2}{c_0}\dfrac{c_1}{c_0}T$	$c_0\dfrac{c_2}{c_0}\dfrac{c_1}{c_0}\dfrac{(2-\phi)\phi}{(1-\phi)^2}$	$c_0\dfrac{c_2}{c_0}\dfrac{c_1}{c_0}\dfrac{T}{1-T},\quad T \le 1$
$M_{2,0}$	$c_1\left(1+\dfrac{c_1}{c_0}T\right)$	$c_1\left(1+\dfrac{c_1}{c_0}\dfrac{(2-\phi)\phi}{(1-\phi)^2}\right)$	$c_1\left(1+\dfrac{c_1}{c_0}\dfrac{T}{1-T}\right),\quad T \le 1$
$M_{0,2}$	$c_2\left(1+\dfrac{c_2}{c_0}T\right)$	$c_2\left(1+\dfrac{c_2}{c_0}\dfrac{(2-\phi)\phi}{(1-\phi)^2}\right)$	$c_2\left(1+\dfrac{c_2}{c_0}\dfrac{T}{1-T}\right),\quad T \le 1$

Note. Solutions for initial condition $c(m, n; 0) = c_1\delta_{m,1} + c_2\delta_{1,n}$. $c_0 = c_1 + c_2$.

sum kernels, all nonzero moments converge on $[0, \infty]$. On the other hand, the two component product kernel has a gel point at $t_g = 1/bc_0$ ($T_g = 1$). As Figs. 8d–8f show, MC simulation successfully reproduces the higher moments for this gelling kernel throughout the radius of convergence of the PBE results. Subsequently, strikingly rapid yet finite increases of the second moments $M_{0,2}$, $M_{1,1}$, and $M_{2,0}$ are observed at the gel point t_g, reflecting the fact that a real system—lacking an infinite number of particles—does not obey Eqs. (49) and (50). Moreover, a single particle of runaway size is observed in the species vector at this point, tantamount to an "infinite gel" of infinitesimal concentration predicted by the deterministic formalism. For $t > t_g$, MC simulation provides new insight into the postgelation period of the process not possible with a PBE. The limiting behavior of Eq. (48) is observed over a decade of dimensionless time, and both components are fully conserved.

As noted in the previous section, the performance of the algorithm depends on the number of species in the state vector, which varies from kernel to kernel. In Fig. 9 we show the maximum number of species formed during discrete simulations of various kernels. In addition to the kernels given by Eqs. (40)–(42), we have included the behavior of the orthokinetic kernel ($K(m, n \mid m', n') \propto ((m + n)^{1/3} + (m' + n')^{1/3})^3$) and the perikinetic kernel, which is discussed at length in the following subsection. As expected, a power-law relationship between $M_{\max}$ and the quantity $\Omega_1\Omega_2$ is observed with an exponent approximately equal to $1/3$, although Eq. (39) gives a more conservative estimate of the coefficient. An unexpected relationship between the maximum number of species and the index of homogeneity λ was observed as well. Noting that the constant and perikinetic kernels ($\lambda = 0$) share the same relationship between $M_{\max}$ and $\Omega_1\Omega_2$ as do the sum and orthokinetic kernels ($\lambda = 1$), the results suggest that as λ increases, so too does $M_{\max}$. Qualitatively, the λ-dependence is a consequence of the capacity of the kernel to direct the aggregation process. Because
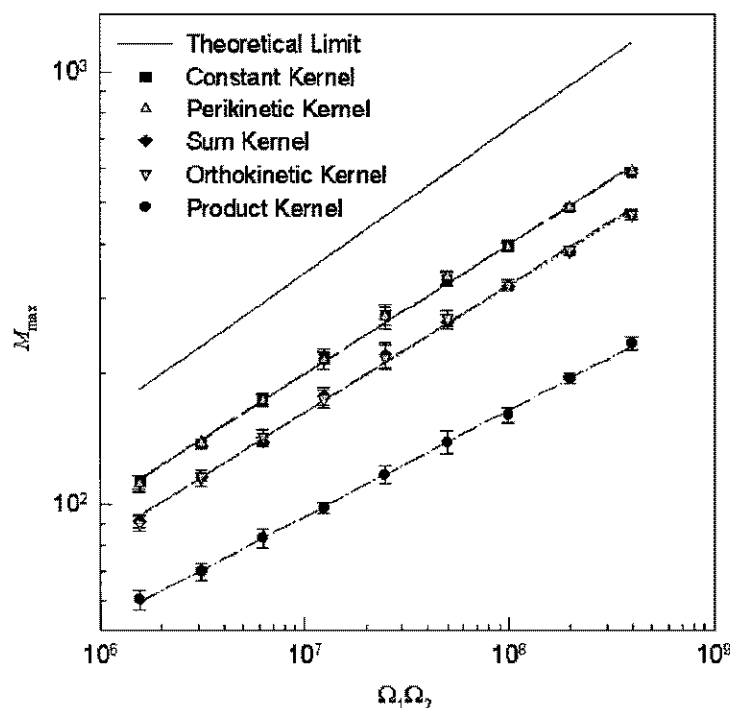
FIG. 9. Maximal number of species possible at one time in a two-component aggregation process initially given Ω_1 monomers of one type and Ω_2 of the other. The theoretical limit is given by Eq. 39.

the perikinetic and constant kernels ($\lambda = 0$) are insensitive to the sizes of the aggregating species, all species are more or less equally prone to aggregate with each other via these kernels. Consequently, this size insensitivity can cause an explosion of singly populated species. In contrast, the product kernel ($\lambda = 2$) strongly favors aggregations of the largest particles—directing the formation of certain species more often than others. The sum and orthokinetic kernels ($\lambda = 1$) fall between these extremes. Because $M_{\max}$ relates directly to the slowest step of the simulation procedure, it follows that the speed of the algorithm increases with λ. Generally speaking, the effects of λ are inconsequential for single-component aggregation, which may be simulated until complete aggregation almost instantaneously for all kernels. This is a consequence of the fact that aggregation products have a smaller species space to occupy, and multiple paths to the same product species are more probable than for multicomponent aggregation.

Finally, as a consequence of species accounting and the aggregation table, the execution speed of the algorithm is competitive with many of the numerical methods used for integration of the PBEs. Typically, simulations of two-component processes with tens of thousands of initial particles required only a few seconds to complete, regardless of the kernel. For all intensive purposes, complete simulations of single-component processes were instantaneous. Much of this is attributable to the aggregation table and its use of partial sums of α. In a comparison of two MC implementations of a two-component continuous aggregation process executed on a 1.2-GHz PC, one using an aggregation table and one without, simulation times for the unoptimized code required 30 min, while the optimized code required only 7s.

4.2. Continuous Processes

Typically, transport-limited aggregation processes require a "continuous" treatment of the composition space, as particles are not "polymers" in the chemical sense. Among the many

kernels for transport-limited processes, one of the most frequently used is the perikinetic kernel describing aggregation that is limited by Brownian motion:

$$K(u_\mu, u_\nu) = \varepsilon_a \frac{2k_B \Theta}{3\eta} \left(\frac{1}{u_\mu^{1/3}} + \frac{1}{u_\nu^{1/3}} \right) \left(u_\mu^{1/3} + u_\nu^{1/3} \right). \tag{51}$$

In Eq. (51), u_μ and u_ν are the total volumes of species μ and ν, k_B is Boltzmann's constant, Θ is the temperature, and η is the viscosity of the suspending medium. The quantity ε_a is the probability that the two particles adhere upon collision. Unfortunately, no exact solution exists for PBEs with this kernel, although approximate or numerical solutions suffice for many applications.

In order to avoid the size dependence of Eq. (51), Smoluchowski [25] observed that it could be approximated by another homogeneous kernel with $\lambda = 0$,

$$K(u_\mu, u_\nu) = \varepsilon_a \frac{8k_B \Theta}{3\eta}. \tag{52}$$

Like Eq. (40), this is a constant kernel with $\beta = \varepsilon_a 8k_B \Theta / 3\eta$. Currently, this is the only kernel for which analytical solution to Lushnikov's equation is possible with a continuous initial distribution density [16]. For an initial distribution with two types of pure, exponentially distributed particles

$$\hat{c}(u, v; 0) = c_1 \lambda_1 e^{-\lambda_1 u} \lambda_2 \delta(\lambda_2 v) + c_2 \lambda_2 e^{-\lambda_2 v} \lambda_1 \delta(\lambda_1 u), \tag{53}$$

we have determined the cumulative size distribution $G(u, v; t)$ resulting from exact solution of Eq. (2) (see Appendix):
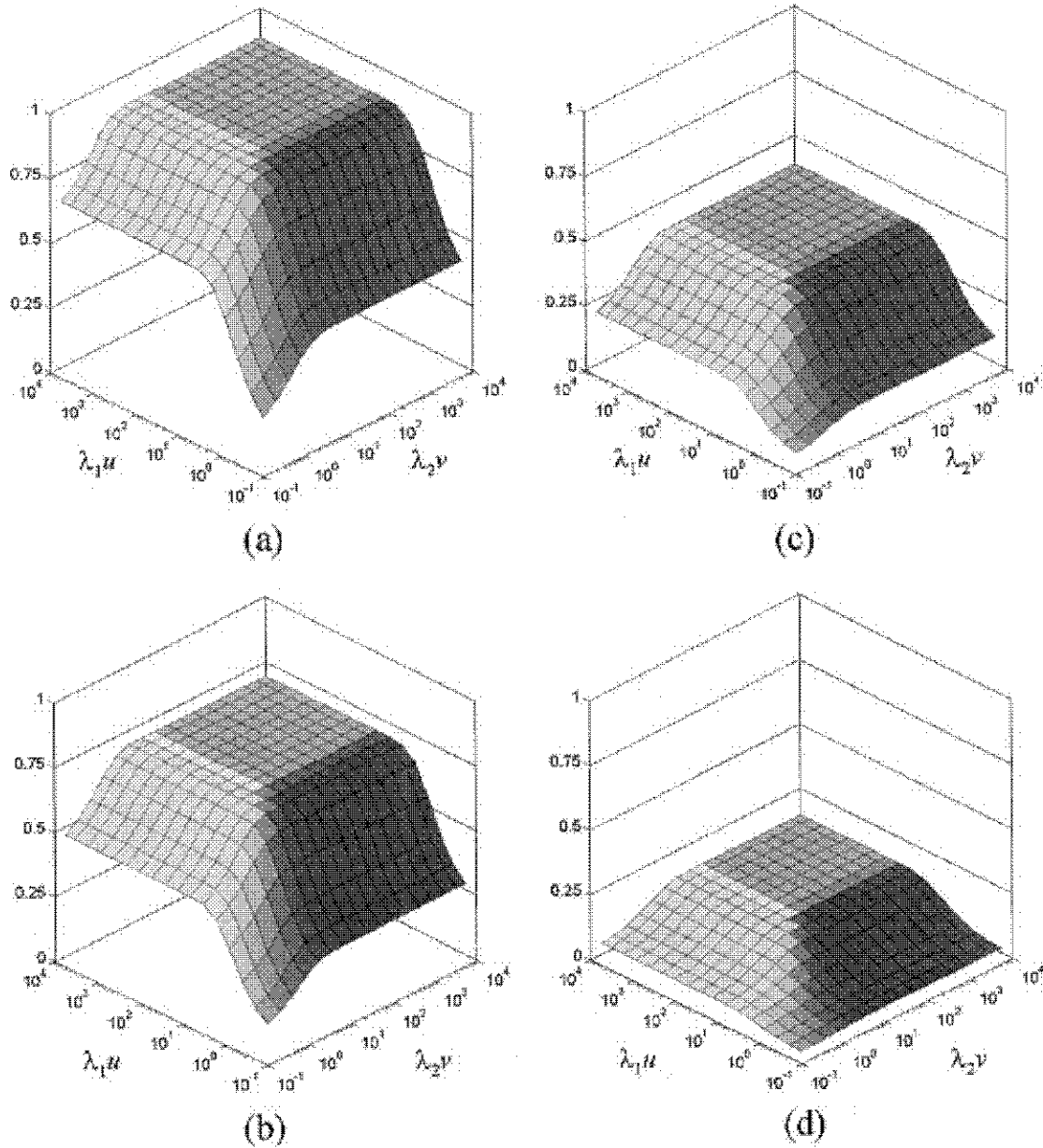
$$\begin{aligned}
G(u, v; t) = \frac{4c_0}{(2+T)^2} &\left\{ \frac{x_1}{\theta_1} \left(1 - e^{-\theta_1 \lambda_1 u} \right) + \frac{x_2}{\theta_2} \left(1 - e^{-\theta_2 \lambda_2 v} \right) \right. \\
&+ \frac{x_1}{\theta_1} \sum_{j=0}^{\infty} \left(\left(\frac{T}{2+T} \right)^2 \frac{x_2 x_1}{\theta_2 \theta_1} \right)^{j+1} P(j+2, \theta_1 \lambda_1 u) P(j+1, \theta_2 \lambda_2 v) \\
&+ \frac{x_2}{\theta_2} \sum_{j=0}^{\infty} \left(\left(\frac{T}{2+T} \right)^2 \frac{x_2 x_1}{\theta_2 \theta_1} \right)^{j+1} P(j+1, \theta_1 \lambda_1 u) P(j+2, \theta_2 \lambda_2 v) \\
&+ \left. \left(\frac{4+2T}{T} \right) \sum_{j=0}^{\infty} \left(\left(\frac{T}{2+T} \right)^2 \frac{x_2 x_1}{\theta_2 \theta_1} \right)^{j+1} P(j+1, \theta_1 \lambda_1 u) P(j+1, \theta_2 \lambda_2 v) \right\}.
\end{aligned} \tag{54}$$

In Eq. (54), $c_0 = c_1 + c_2$ is the initial concentration of particles, $T = \beta c_0 t$ is a dimensionless time scale, $P(a, x)$ is the incomplete gamma function [1], and x_i and θ_i are given by

$$x_i = \frac{c_i}{c_0}, \quad i = 1, 2, \tag{55}$$

and

$$\theta_i = 1 - \left(\frac{T}{2+T} \right) x_i, \quad i = 1, 2. \tag{56}$$
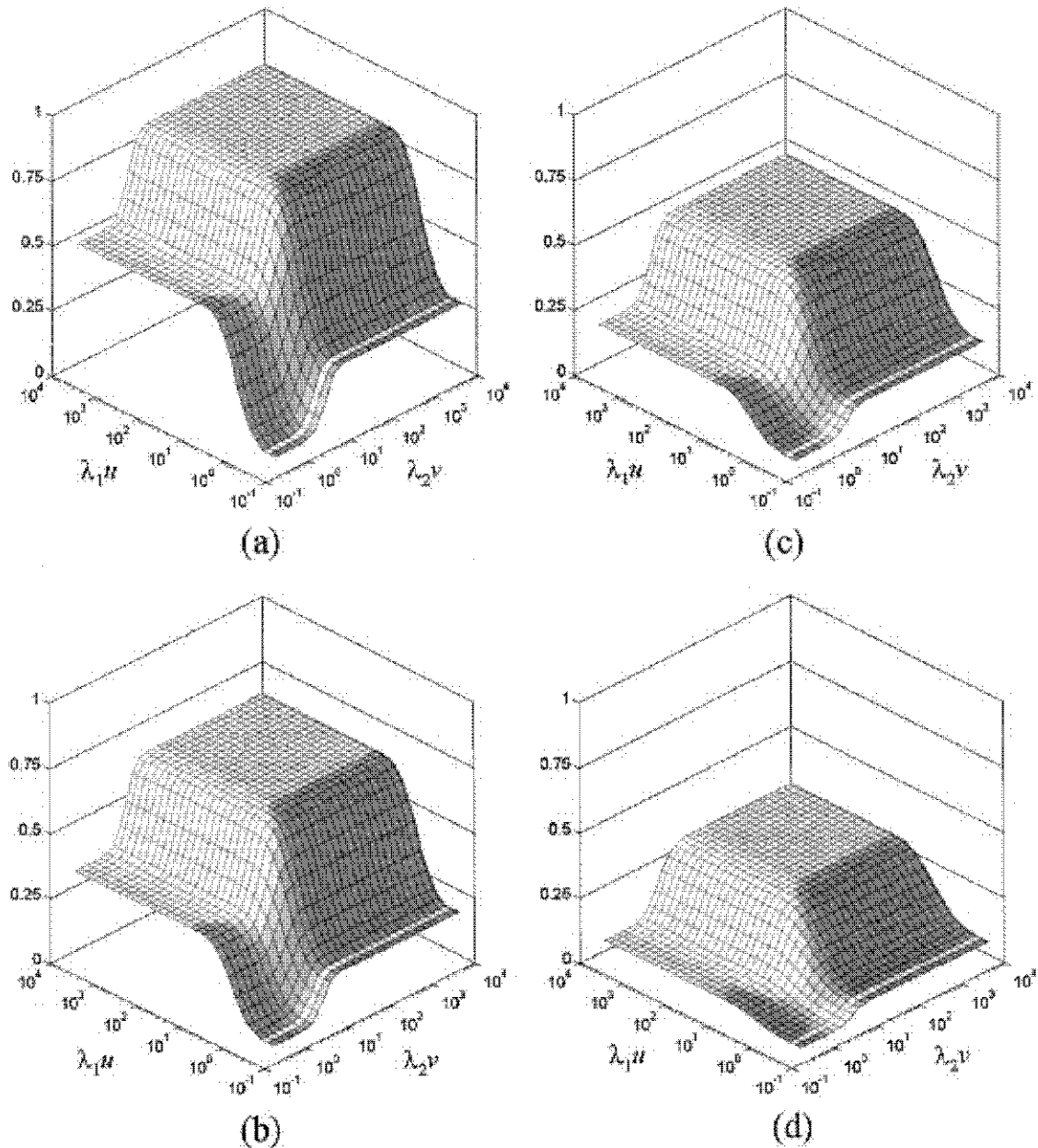
FIG. 10. Normalized, MC-generated cumulative particle size distributions $G(u, v; T)/G(\infty, \infty; 0)$ at dimensionless times (a) $T = 3.8 \times 10^3$, (b) $T = 1.3 \times 10^4$, (c) $T = 4.7 \times 10^4$, and (d) $T = 1.6 \times 10^5$ ($T = \beta c_0 t$) for a constant kernel.

Results of simulations with the parameters $c_1 = 10000$, $c_2 = 5000$, $\lambda_1 = 0.25$, $\lambda_2 = 0.125$, $\beta = 1$, and $V = 1$ (with discretization $\mathcal{M}_1 = \mathcal{M}_2 = 50$) are given in Fig. 10. For all choices of parameters for the initial distribution, the analytical solution of Lushnikov's equation and results of MC simulations were virtually indistinguishable from each other. Kolmogorov–Smirnov significance testing [19] strongly indicated that the distributions resulting from Lushnikov's equation and *individual* MC simulations were not statistically different, with P-values ranging from 0.7 to 1 at each time point. Despite the natural variation from one simulation to the next, we found that averaging the results of several MC simulations was unnecessary as long as the initial number of particles in the simulation was large and the discretization sufficiently fine. In part, this is due to the summation over the species in Eq. (26), which acts as a type of species averaging. If the concentration density $\hat{c}(u, v; t)$ is desired, several sets of simulation results must be performed so as to make the surface $G(u, v; t)$ conducive to numerical differentiation.

In addition to the simulations of a process with a constant kernel, we have also computed the time evolution of a Brownian aggregation using Eq. (51). For purposes of demonstration, we include a composition-dependent sticking probability $\varepsilon_a(y_\mu, y_\nu)$ in order to introduce composition dependence into the size-insensitive kernel. Consider the sticking probabilities between pure particles of two different components $\varepsilon_{1,1}$, $\varepsilon_{2,2}$, and $\varepsilon_{1,2}$. If adhesion between two aggregates is mediated by a single point of contact, the equation that can be used to describe the heterotypic sticking probability is

$$\varepsilon_a(u_\mu, u_\nu) = (y_\mu y_\nu)\varepsilon_{1,1} + ((1 - y_\mu)y_\nu + y_\mu(1 - y_\nu))\varepsilon_{1,2} + (1 - y_\mu)(1 - y_\nu)\varepsilon_{2,2}, \quad (57)$$

where y_μ and $(1 - y_\mu)$ are the volumetric fractions of the first and second components in

FIG. 11.   Normalized cumulative particle size distributions $G(u, v; T)/G(\infty, \infty; 0)$ at dimensionless times (a) $t^* = 0.197$, (b) $t^* = 0.441$, (c) $t^* = 0.989$, and (d) $t^* = 2.21$, where $t^* = c_0(2k\Theta/3\eta)t$. Simulations represent Brownian aggregation of nanoscopic particles in water at $\Theta = 293$ K with a particle volume fraction of approximately 1%.

species μ. We note that with increased information of aggregate morphology, such as the distribution of the numbers of points of contact, more complex forms of ε_a are possible. Using this model of the composition dependence of the perikinetic kernel, we conducted simulations of 15,000 particles in a volume of $V = 2.30 \times 10^{-8}$ ml. As in the previous example, the initial concentration density was chosen to reflect the aggregation of two initially pure sets of particles with unique size distributions, in this case gamma,

$$\hat{c}(u, v; 0) = c_1 \frac{\lambda_1 (\lambda_1 u)^{\sigma_1 - 1} e^{-\lambda_1 u}}{\Gamma(\sigma_1)} \lambda_2 \delta(\lambda_2 v) + c_2 \frac{\lambda_2 (\lambda_2 v)^{\sigma_2 - 1} e^{-\lambda_2 v}}{\Gamma(\sigma_2)} \lambda_1 \delta(\lambda_1 u), \qquad (58)$$

with $\sigma_1 = 2.0$, $\sigma_2 = 6.0$, $\lambda_1 = 4.78 \times 10^{-10}$ ml^{-1}, and $\lambda_2 = 1.59 \times 10^{-10}$ ml^{-1}. The respective concentrations of the initial particles were $c_1 = 4.34 \times 10^{11}$ particles/ml and $c_2 = 2.17 \times 10^{11}$ particles/ml, and the composition spaces were discretized such that $\mathcal{M}_1 = \mathcal{M}_2 = 50$. Furthermore, we assumed the suspending medium to be water at $\Theta = 293$ K, such that $(2k_B \Theta / 3\eta) = 2.70 \times 10^{-9}$ ml/s. The sticking probabilities were taken as $\varepsilon_{1,1} = 0.8$, $\varepsilon_{2,2} = 0.1$, and $\varepsilon_{1,2} = 0.6$, representing a situation whereby heterotypic aggregation is preferred for the second component, but not necessarily the first. We show the results of the simulation in Fig. 11. The relative asymptotic values of the cumulative distribution as $u \to 0$ and $v \to 0$ reflect the disparity of the two initial particle concentrations, and as time increases, the consumption of the pure particles is reflected in their relative decrease. Figure 11a shows that even after about 20% of the initial particles have aggregated, the relative amounts of pure particles are virtually unchanged. Subsequently, the relative populations of the pure particles equalize as the distribution becomes more symmetric. This behavior contrasts with that of the constant kernel (Fig. 10), which more or less maintains the population ratio of pure particles until complete aggregation. The differences between the two kernels are functions of both the promotion of size-disproportionate events by Eq. (51) and the favoring of aggregation of type 1 particles by Eq. (58).

5. DISCUSSION

By treatment of multicomponent aggregation processes akin to copolymerization, we have proposed an efficient and exact MC simulation algorithm based upon Gillespie's implementation of the stochastic approach to chemical kinetics [7]. In addition to providing a means of simulating aggregation and polymerization processes with any number of components in a robust manner, the algorithm can reproduce the results of multicomponent PBEs within the radii of convergence of their solutions and extends these results to times where the PBE approach is potentially unreliable. Moreover, MC simulation permits statistical analyses of the inherent statistical fluctuations of multicomponent aggregation processes not possible using deterministic techniques.

As discussed in Section 2, our MC algorithm is microphysically equivalent to the exact MC algorithms of Gillespie [6] and Shah *et al.* [23] for particle coalescence. We denote these algorithms as particle accounting, as they keep track of each particle in the simulation. By using a chemical interpretation to define the state of an aggregating system in terms of "aggregate species," the bookkeeping of the stochastic simulation may be significantly improved. While particle accounting algorithms require $O(\Omega_1 + \Omega_2 + \ldots \Omega_\kappa)$ numerical operations per time step where $\{\Omega_k\}$ are the total amounts of each component $k \in [1, \kappa]$, our species accounting algorithm requires only $O((\Omega_1 \Omega_2 \ldots \Omega_\kappa)^{1/(\kappa+1)})$ numerical operations per time step. Moreover, the storage requirements of our species accounting algorithm are

at most $O((\Omega_1 \Omega_2 \ldots \Omega_\kappa)^{2/(\kappa+1)})$, while particle accounting algorithms require $O((\Omega_1 + \Omega_2 + \ldots \Omega_\kappa)^2)$. For kernels that are not homogeneous with respect to time, the number of operations per time step squares for both implementations, bringing about even more dramatic relative improvements for our species accounting algorithm.

The algorithm itself follows. A set of initial aggregate species are defined as types of particles with specific compositions. Subsequently, the time until the next aggregation event and the species involved are selected by MC using a microphysically exact "aggregation probability density function." After updating the populations of the involved species and the time, the process is repeated until some predefined time or event. By use of this procedure, aggregation processes governed by any kernel can be exactly simulated from any initial condition all the way through complete aggregation.

The bookkeeping of the algorithm can be dramatically simplified by use of an "aggregation table," which optimizes the bookkeeping of species and their probabilities of aggregation with each other. In addition to simplifying the creation, update, and destruction of species in the state vector, the aggregation table simplifies the use and update of the partial sums $\{\alpha_\mu\}$ used in the selection of aggregating species and the quiescence times. In practice, this translates to hundredfold increases in execution speed over implementations without the use of the partial sums. As a consequence, most simulations of discrete processes with tens of thousands of particles require at most a few seconds of computation to reach complete aggregation, whereas continuous processes can take longer. These ultrafast run times facilitate interactive deconvolution algorithms for the determination of kernels from size-composition distribution data sets.

In the study of some representative aggregation processes, we showed that the stochastic and deterministic formalisms are equivalent in the limit of large initial populations and times preceding complete aggregation. For processes with kernels featuring a gel transition, the results of MC simulation and the PBE agree within the interval $t \in [0, t_g]$. For many applications within these time limits, numerical integration methods for PBEs [10, 11, 13, 14] or their moments [32] may be sufficient alternatives. However, MC implementation of the stochastic approach is the only means of exactly predicting the complete time evolution of all multicomponent aggregation processes. In conclusion, owing to the speed and exactness of this approach, we believe it to have many useful applications to a broad range of physically relevant problems.

APPENDIX

Lushnikov's solution to Eq. (5) for the constant kernel is expressed in terms of the double Laplace transform of $\hat{c}(u, v; T)$, defined by

$$\phi(p, q; T) = \frac{1}{c_0} \int\limits_0^\infty \int\limits_0^\infty e^{-pu-qv} \hat{c}(u, v; T) \, du \, dv, \tag{A.1}$$

where $T = \beta c_0 t$ and $c_0 = \int_0^\infty \int_0^\infty \hat{c}(u, v; 0) \, du \, dv$. The Laplace space solution to Eq. 2 is [16]

$$\phi(p, q; T) = \frac{4}{2+T} \frac{\phi(p, q; 0)}{2+T-T\phi(p, q; 0)}. \tag{A.2}$$

This solution may be inverted given $\phi(p, q; 0)$, which follows directly from Eq. (53) as

$$\phi(p, q; 0) = x_1\lambda_1 \frac{1}{p + \lambda_1} + x_2\lambda_2 \frac{1}{p + \lambda_2}, \tag{A.3}$$

where $x_i = c_i/c_0$. Substituting (A.3) into (A.2) yields, after some rearrangement, the expression

$$\phi(p, q; T) = \frac{x_2\lambda_2\left(\frac{2}{2+T}\right)^2}{(q + \lambda_2 v_2)}\left(1 + \frac{\left(\frac{(q+\lambda_2)x_1\lambda_1}{x_2\lambda_2} + \left(\frac{T}{2+T}\right)\frac{(q+\lambda_2)x_1\lambda_1}{(q+\lambda_2 v_2)}\right)}{p + \left(\left(\frac{T}{2+T}\right)\frac{(q+\lambda_2)x_1\lambda_1}{(q+\lambda_2 v_2)}\right)}\right), \tag{A.4}$$

where we have defined $v_2 = 1 - (\frac{T}{2+T})x_2$. Finally, using standard Laplace inverse transform tables [1] and the relationship

$$\frac{1}{2\pi i}\oint e^{st}e^{\frac{k}{s}}\,ds = \frac{1}{2\pi i}\oint e^{st}\left(1 + \sum_{j=1}^{\infty}\frac{(k/s)^j}{j!}\right)ds$$

$$= \delta(t) + k\sum_{j=0}^{\infty}\frac{1}{j!}\frac{(kt)^j}{(j+1)!}$$

$$= \delta(t) + k\frac{I_1(2\sqrt{kt})}{\sqrt{kt}}, \tag{A.5}$$

the two-component concentration density $\hat{c}(u, v; T)$ may be expressed as

$$\hat{c}(u, v; T) = \frac{4c_0\lambda_1\lambda_2}{(2+T)^2}\left\{x_1\delta(\lambda_2 v)e^{-\lambda_1 v_1 u} + x_2\delta(\lambda_1 u)e^{-\lambda_2 v_2 v}\right.$$

$$+ 2x_1 x_2 I_0\left(2\left(\frac{t}{2+T}\right)\sqrt{(x_1\lambda_1 u)(x_2\lambda_2 v)}\right)e^{-\lambda_1 v_1 u - \lambda_2 v_2 v}$$

$$+ \left[x_1 x_2 e^{-\lambda_1 v_1 u - \lambda_2 v_2 v}\left(\sqrt{\frac{x_1\lambda_1 u}{x_2\lambda_2 v}} + \sqrt{\frac{x_2\lambda_2 v}{x_1\lambda_1 u}}\right)\right.$$

$$\left.\left.\times I_1\left(2\left(\frac{T}{2+T}\right)\sqrt{(x_1\lambda_1 u)(x_2\lambda_2 v)}\right)\right]\right\}, \tag{A.6}$$

where $v_1 = 1 - (\frac{T}{2+T})x_1$ and $I_n(x)$ is the modified Bessel function [1].

In order to compute the cumulative composition distribution $G(u, v; t)$, the identity

$$\frac{I_v(2\sqrt{z})}{(\sqrt{z})^v}\Gamma(v + 1) = (v - 1)!\sum_{j=0}^{\infty}\frac{1}{(v + j)!}\frac{z^j}{j!} \tag{A.7}$$

may be used, turning (A.6), after some rearrangement, into

$$\hat{c}(u, v; T) = \frac{4c_0\lambda_1\lambda_2}{(2+T)^2}\left\{x_1\delta(\lambda_2 v)e^{-\lambda_1 v_1 u} + x_2\delta(\lambda_1 u)e^{-\lambda_2 v_2 v}\right.$$

$$+ \sum_{j=0}^{\infty}\left(\left(\frac{T}{2+T}\right)^2 x_1 x_2\right)^{j+1}e^{-\lambda_1 v_1 u - \lambda_2 v_2 v}\left[2\left(\frac{2+T}{T}\right)\frac{(\lambda_1 u)^j}{j!}\frac{(\lambda_2 v)^j}{j!}\right.$$

$$\left.\left.+ x_1\frac{(\lambda_2 v)^j}{j!}\frac{(\lambda_1 u)^{j+1}}{(j+1)!} + x_2\frac{(\lambda_2 v)^{j+1}}{(j+1)!}\frac{(\lambda_1 u)^j}{j!}\right]\right\}. \tag{A.8}$$

Equation (54) follows by double integration of (A.8) using the definition of the incomplete gamma function

$$P(a, x) = \frac{1}{\Gamma(a)} \int_0^x x^{a-1} e^{-x} \, dx. \tag{A.9}$$

ACKNOWLEDGMENTS

REFERENCES

1. M. Abramowitz and I. A. Stegun, *Handbook of Mathematical Functions* (Dover, New York, 1972).

2. M. H. Bayewitz, J. Yerushalmi, S. Katz, and R. Shinnar, The extent of correlations in a stochastic coalescence process, *J. Atmos. Phys.* **31**, 1604 (1974).

3. S. K. Friedlander, *Smoke, Dust and Haze* (Oxford University Press, New York, 2000).

4. F. M. Gelbard and J. H. Seinfeld, Coagulation and growth of a multicomponent aerosol, *J. Colloid Interface Sci.* **63**, 472 (1978).

5. D. T. Gillespie, The stochastic coalescence model for cloud droplet growth, *J. Atmos. Sci.* **29**, 1496 (1972).

6. D. T. Gillespie, An exact method for numerically simulating the stochastic coalescence process in a cloud, *J. Atmos. Sci.* **32**, 1977 (1975).

7. D. T. Gillespie, A general method for numerically simulating the stochastic time evolution of coupled chemical reactions, *J. Comput. Phys.* **22**, 304 (1976).

8. A. M. Golovin, The solution of the coagulation equation for cloud droplets in a rising air current, *Izv. Zkad. Nauk. SSSR Ser. Geofiz.* **5**, 482 (1963).

9. E. M. Hendriks, J. L. Spouge, M. Eibl, and M. Schreckenberg, Exact solutions for random coagulation processes, *Z. Phys. B Condens. Matter* **58**, 219 (1985).

10. M. J. Hounslow, R. L. Ryall, and V. R. Marshall, A discretized population balance for nucleation, growth, and aggregation, *AIChE J.* **34**, 1821 (1988).

11. N. Kourti and A. Schatz, Solution of the general dynamic equation (GDE) for multicomponent aerosols, *J. Aerosol Sci.* **21**, 41 (1998).

12. P. L. Krapivsky and E. Ben-Naim, Aggregation with multiple conservation laws, *Phys. Rev. E.* **53**, 291 (1996).

13. S. Kumar and D. Ramkrishna, On the solution of population balance equations by discretization. I. A fixed pivot technique, *Chem. Eng. Sci.* **51**, 1311 (1996).

14. S. Kumar and D. Ramkrishna, On the solution of population balance equations by discretization. II. A moving pivot technique, *Chem. Eng. Sci.* **51**, 1333 (1996).

15. I. J. Laurenzi and S. L. Diamond, Monte Carlo simulation of the heterotypic aggregation kinetics of platelets and neutrophils, *Biophys. J.* **77**, 1733 (1999).

16. A. A. Lushnikov, Evolution of coagulating systems. III. Coagulating mixtures, *J. Colloid Interface Sci.* **54**, 94 (1976).

17. A. A. Lushnikov, Coagulation in finite systems, *J. Colloid Interface Sci.* **65**, 276 (1978).

18. J. B. McLeod, On an infinite set of non-linear differential equations, *Q. J. Math. Oxford* **2**, 119 (1962).

19. W. H. Press, S. A. Teukolsky, W. T. Vetterling, and B. P. Flannery, *Numerical Recipes in C* (Cambridge University Press, Cambridge, UK, 1992).

20. D. Ramkrishna and J. D. Borwanker, A puristic analysis of population balance. I, *Chem. Eng. Sci.* **28**, 1423 (1973).

21. D. Ramkrishna, B. H. Shah, and J. D. Borwanker, Analysis of population balance. III. Agglomerating populations, *Chem. Eng. Sci.* **31**, 435 (1976).

22. A. Rényi, A discussion of chemical reactions using the theory of stochastic processes, *MTA Alk. Mat. Int. Közl.* **2**, 83 (1953).

23. B. H. Shah, D. Ramkrishna, and J. D. Borwanker, Simulation of particulate systems using the concept of the interval of quiescence, *AIChE J.* **23**, 897 (1977).

24. M. Smith and T. Matsoukas, Constant-number Monte Carlo simulation of population balances, *Chem. Eng. Sci.* **53**, 1777 (1998).

25. M. v. Smoluchowski, Vensuch einer mathematischen theorie der koagulationkinetic kolloider lösungen, *Z. Phys. Chem.* **92**, 129 (1917).

26. J. L. Spouge, Monte-Carlo results for random coagulation, *J. Colloid Interface Sci.* **107**, 38 (1985).

27. H. Tanaka and K. Nakazawa, Stochastic coagulation equation and validity of the statistical coagulation equation, *J. Geomeg. Geoelectr.* **45**, 361 (1993).

28. H. Tanaka and K. Nakazawa, Validity of the statistical coagulation equation and runaway growth of proto-planets, *Icarus* **107**, 404 (1994).

29. P. Tandon and S. L. Diamond, Hydrodynamic effects and receptor interactions of platelets and their aggregates in linear shear flow, *Biophys. J.* **73**, 2819 (1997).

30. M. Thorn, H. P. Breuer, F. Petruccione, and J. Honerkamp, A master equation investigation of coagulation reactions—Sol-gel transition, *Makromol. Chem. Theory. Simul.* **3**, 585 (1994).

31. R. D. Vigil and R. M. Ziff, On the scaling theory of two-component aggregation, *Chem. Eng. Sci.* **53**, 1725 (1998).

32. D. L. Wright, R. McGraw, and D. E. Rosner, Bivariate extension of the quadrature method of moments for modeling simultaneous coagulation and sintering of particle populations, *J. Colloid Interface Sci.* **236**, 242 (2001).

33. R. M. Ziff, Kinetics of polymerization, *J. Stat. Phys.* **23**, 241 (1980).